FtsK is Critical for the Assembly of the Unique Divisome Complex of the FtsZ-less *Chlamydia trachomatis*

Authors: McKenna Harpring[1], Junghoon Lee[2], Guangming Zhong[3], Scot P. Ouellette[2], and John V. Cox[1*]

Affiliations: Department of Microbiology, Immunology, and Biochemistry. University of Tennessee Health Science Center. Memphis, TN, USA[1], Department of Pathology, Microbiology, and Immunology, University of Nebraska Medical Center, Omaha, NE, USA[2], Department of Microbiology, Immunology, and Molecular Genetics, University of Texas Health San Antonio, TX, USA[3]

*** Correspondence:**
Corresponding Author: John V. Cox
jcox@uthsc.edu

Abstract:

Chlamydia trachomatis serovar L2 *(Ct),* an obligate intracellular bacterium that does not encode FtsZ, divides by a polarized budding process. In the absence of FtsZ, we show that FtsK, a chromosomal translocase, is critical for divisome assembly in *Ct*. Chlamydial FtsK forms discrete foci at the septum and at the base of the progenitor mother cell, and our data indicate that FtsK foci at the base of the mother cell mark the location of nascent divisome complexes that form at the site where a daughter cell will emerge in the next round of division. The divisome in *Ct* has a hybrid composition, containing elements of the divisome and elongasome from other bacteria, and FtsK is recruited to nascent divisomes prior to the other chlamydial divisome proteins assayed, including the PBP2 and PBP3 transpeptidases, and MreB and MreC. Knocking down FtsK prevents divisome assembly in *Ct* and inhibits cell division and septal peptidoglycan synthesis. We further show that MreB does not function like FtsZ and serve as a scaffold for the assembly of the *Ct* divisome. Rather, MreB is one of the last proteins recruited to the chlamydial divisome, and it is necessary for the formation of septal peptidoglycan rings. Our studies illustrate the critical role of chlamydial FtsK in coordinating divisome assembly and peptidoglycan synthesis in this obligate intracellular bacterial pathogen.

Word count: 221

38 **Introduction**

39 Most bacteria divide by a highly conserved process termed binary fission, which occurs
40 through the symmetric division of the parental cell into two daughter cells (Harpring 2023).
41 However, *Chlamydia trachomatis* serovar L2 (*Ct*), a coccoid, gram-negative, obligate
42 intracellular bacterium divides by a polarized cell division process characterized by an
43 asymmetric expansion of the membrane from one pole of a coccoid cell resulting in the
44 formation of a nascent daughter cell (Abdelrahman 2016; Ouellette SP 2022).

45 *Ct* undergoes a biphasic developmental cycle during infection. Non-replicating and
46 infectious elementary bodies (EBs) bind to and are internalized by target cells. Following
47 internalization, EBs within a membrane vacuole, termed the inclusion, differentiate into
48 replicating reticulate bodies (RBs). After replication, RBs undergo secondary differentiation into
49 EBs, which are released from cells to initiate another round of infection (Abdelrahman 2005).

50 In evolving to obligate intracellular dependence, *Ct* has eliminated several gene products
51 essential for cell division in other bacteria, including the central coordinator of divisome
52 formation, FtsZ (Stephens 1998; Ouellette SP 2020). This tubulin-like protein forms filaments
53 that associate to form a ring at the division plane (Barrows 2021), which serves as a scaffold for
54 the assembly of the other components of the bacterial divisome that regulate the processes of
55 septal peptidoglycan (PG) synthesis and chromosomal translocation. Of the twelve divisome
56 proteins shown to be essential for cell division in the model gammaproteobacterial organism, *E.*
57 *coli, Ct* encodes homologues of FtsK, a chromosomal translocase (Ouellette SP 2012); FtsQLB,
58 regulators of septal PG synthesis (Ouellette SP 2015; Kaur 2022), FtsW, a septal
59 transglycosylase (Putman T 2019), and penicillin binding protein 3 (PBP3/FtsI), a septal
60 transpeptidase (Ouellette SP 2012).

61 In addition to the divisome, rod-shaped bacteria employ another multiprotein complex, the
62 elongasome, which directs sidewall PG synthesis (Liu 2020) necessary for cell lengthening and
63 the maintenance of cell shape prior to division. Although *Ct* is a coccoid organism, it encodes
64 several elongasome proteins, including MreB, MreC, RodA, RodZ, and penicillin binding
65 protein 2 (PBP2), a sidewall transpeptidase (Ouellette SP 2012; Ouellette SP 2014; Cox 2020).
66 The actin-like protein MreB is essential for cell division (Ouellette SP 2012; Abdelrahman 2016)
67 and forms septal rings in *Ct* (Kemege 2015; Liechti 2016; Lee 2020). These observations led to
68 the proposal that MreB replaces FtsZ in *Ct* and serves as a scaffold necessary for the assembly of
69 the chlamydial divisome (Lee 2020).
70 While inhibitor studies suggest that chlamydial cell division is dependent upon elements of
71 the divisome and elongasome from other organisms (Ouellette SP 2012; Abdelrahman 2016; Cox
72 2020), the composition and ordered assembly of the chlamydial divisome and its distribution
73 during polarized budding are undefined. We hypothesized that FtsK, a chromosomal translocase,
74 serves a critical function in regulating the division process of *Ct,* given previous observations
75 demonstrating it interacts with elements of both the elongasome and divisome (Ouellette SP
76 2012). We show here that FtsK is critical for the assembly of the hybrid divisome complex of *Ct*
77 and that MreB does not serve as a scaffold necessary for the assembly of the chlamydial
78 divisome. Rather, chlamydial MreB associates with this hybrid divisome complex late in the
79 chlamydial divisome assembly process, and MreB filament formation is necessary for the
80 formation of septal PG rings. Therefore, our data identify FtsK as a key regulator of the cell
81 division process of *Ct*.
82

83 **Results**

84 **FtsK Forms Foci in *Ct* that Mark the Location of Divisome Complexes**

85 In the *E. coli* linear divisome assembly pathway (Du 2017), FtsK is the first protein
86 downstream of FtsZ encoded by *Ct* (Figure 1A). In other organisms, FtsK is uniformly
87 distributed at the septum of dividing cells (Yu 1998; Wang 2006; Veiga 2017). To investigate the
88 localization of FtsK during cell division in *Ct*, HeLa cells were infected with *Ct*. To overcome
89 the challenges associated with assessing cell morphologies in densely packed inclusions in
90 infected cells, we analyzed FtsK localization in *Ct* derived from lysates of infected HeLa cells at
91 21 hrs post-infection (hpi) as described previously (Ouellette SP 2022). *Ct* were stained with an
92 antibody against the chlamydial major outer membrane protein (MOMP) and an antibody that
93 recognizes endogenous FtsK. Blotting analysis revealed that this FtsK antibody recognizes a
94 single protein with the predicted molecular mass of FtsK (Supp. Fig. S1A). Our results showed
95 that, unlike FtsK in other organisms, chlamydial FtsK accumulates in discrete foci in the
96 membrane of coccoid cells (Fig. 1B). In cell division intermediates, FtsK localized in foci at the
97 septum, foci at the septum and at the base of the progenitor mother cell, or foci at the base of the
98 progenitor mother cell only (Figure 1C). The chlamydial FtsK foci observed during cell division
99 were not uniformly distributed at the septum, rather septal foci of FtsK were restricted to one
100 side of the MOMP-stained septum. In addition, the FtsK foci were often above or below (marked
101 with arrowheads in Fig. 1C) the MOMP-stained septum. Similar analyses were performed using

102 *Ct* transformed with the pBOMB4-Tet (-GFP) plasmid encoding FtsK with a C-terminal
103 mCherry tag. The expression of this mCherry fusion is under the control of an
104 anhydrotetracycline (aTc)-inducible promoter. HeLa cells were infected with the transformant,
105 and the expression of the fusion was induced by the addition of 10nM aTc to the media of
106 infected cells at 19hpi. RBs were harvested from the induced cells at 21hpi and stained with
107 MOMP antibodies. Imaging analyses revealed that like endogenous FtsK, FtsK-mCherry
108 accumulated in foci in coccoid cells (Fig. 1D), and in division intermediates, it localized in foci
109 at the septum, foci at the septum and at the base of the progenitor mother cell, or foci at the base
110 of the progenitor mother cell only (Fig. 1E). The foci of FtsK-mCherry, like endogenous FtsK,
111 were often offset relative to the plane defined by MOMP staining at the septum (arrowhead in
112 Fig. 1E). Inclusion forming unit (IFU) assays demonstrated that overexpression of the FtsK-
113 mCherry fusion had no effect on chlamydial developmental cycle progression and the production
114 of infectious EBs (Supp. Fig. S2A). While it is possible that the population of FtsK at the base of
115 the mother cell is a remnant of FtsK from a previous division, ~20% of dividing cells have a
116 secondary bud (Fig. 1F), and FtsK and FtsK-mCherry accumulate in foci at the base of
117 secondary buds (arrowheads in Fig. 1G), suggesting that the population of FtsK at the base of the
118 mother cell corresponds to a nascent divisome complex that forms at the site where the daughter
119 cell will arise in the next round of division.

120 To investigate the distribution of other putative chlamydial divisome components during
121 budding, we transformed *Ct* with plasmids encoding PBP2, PBP3, or MreC with an N-terminal
122 mCherry tag. IFU assays demonstrated that the aTc induced overexpression of the PBP2, PBP3,
123 and MreC fusions had no effect on the developmental cycle progression of *C*t (Supp. Fig. S2A).
124 In addition, blotting analyses revealed that mCherry antibodies primarily detected single species
125 with the predicted molecular mass of the FtsK, PBP2, PBP3, and MreC fusions in lysates
126 prepared from induced cells (Supp. Fig. S1B). The PBP2, PBP3, and MreC fusions were induced
127 by the addition of 10nM aTc to infected cells at 19hpi, and the induced cells were harvested at
128 21hpi and stained with MOMP antibodies. Imaging analyses revealed that the PBP2, PBP3, and
129 MreC fusions accumulated in foci in coccoid cells (Fig. 2A), and in cell division intermediates,
130 the fusions accumulated in foci at the septum, in foci at the septum and at the base of the
131 progenitor mother cell, or in foci only at the base of the progenitor mother cell (Fig. 2B). Similar
132 analyses with an MreB_6xHis fusion (Lee 2020) revealed that MreB exhibited a similar
133 localization profile (Figs. 2A and B). Each of these fusions, like FtsK, were restricted to one side
134 and were often slightly above or slightly below (marked with arrowheads in Fig. 2B) the
135 MOMP-stained septum in dividing cells. The foci of the fusions were also detected at the base of
136 secondary buds (arrowheads in Supp. Fig. S2B). Quantification of the localization profiles of
137 endogenous FtsK and the various fusion proteins revealed that the distribution profile of FtsK-
138 mCherry accurately reflected the distribution of endogenous FtsK (Fig. 2C). Furthermore, a

139 greater percentage of FtsK was associated with the base of dividing cells (including cells with
140 septum and base, and cells with base alone) suggesting that FtsK associates with nascent
141 divisomes at the base of dividing cells prior to the other putative divisome proteins assayed.
142 Finally, this analysis suggested that MreB associated with nascent divisomes at the base of
143 dividing cells after mCherry-PBP2 and mCherry-PBP3 (marked with # in Fig. 2C). The
144 localization profiles of the chlamydial divisome proteins (Figs. 1 and 2) likely reflect the
145 assembly of divisome complexes at the septum and at the base of the progenitor mother cell, and
146 the disassembly of the septal divisome when divisome proteins are only present at the base of the
147 mother cell.

148 Since it was possible that the localization profiles of the mCherry-PBP2 and mCherry-PBP3
149 fusions were at least in part due to their induced over-expression, we performed similar studies
150 with rabbit antibodies generated against peptides derived from PBP2 or PBP3 (Ouellette SP
151 2012). Blotting analyses (Supp. Fig. S1C) with these antibodies revealed that they recognized
152 mCherry-PBP2 and mCherry-PBP3 in *Ct* lysates, and immunofluorescent staining with the PBP2
153 and PBP3-specific antibodies (Supp. Fig. S1D) completely overlapped the mCherry fluorescence
154 in cells when the mCherry PBP2 and PBP3 fusions were inducibly expressed in *Ct*. Imaging
155 analyses with the antibodies that recognize endogenous PBP2 and endogenous PBP3 indicated
156 that these antisera detected foci in coccoid cells, and in cell division intermediates, the PBP2 and
157 PBP3 antibodies detected foci at the septum, foci at the septum and at the base of the mother cell,

158 or foci at the base alone (Supp. Fig. S3A). Quantification revealed that the localization profiles
159 of endogenous PBP2 and PBP3 in division intermediates (Supp. Fig. S3B) were not statistically
160 different than the localization profiles observed for the mCherry fusions of PBP2 and PBP3 (Fig.
161 2C).

162 The quantification in Fig. 2C suggested that FtsK is recruited to nascent divisomes that form
163 at the base of dividing cells prior to the other divisome components assayed. This hypothesis was
164 tested by staining cells expressing the PBP2, PBP3, MreC, or MreB fusions with antibodies that
165 recognize endogenous FtsK. Imaging analyses revealed that in a subset of cells, FtsK was
166 detected in foci at the septum and at the base of dividing cells, while each of the fusions was only
167 detected at the septum where they overlapped the distribution of septal FtsK (Fig. 2D), indicating
168 that FtsK is recruited to nascent divisomes at the base of the cell prior to the other divisome
169 components assayed. Additional analyses revealed that FtsK also overlapped the distribution of
170 the PBP2, PBP3, MreC, and MreB fusions following their appearance at the base of dividing
171 cells (Supp. Fig. S4A). Quantification revealed the percentage of cells in which FtsK overlapped
172 the distribution of each of the fusions at the septum, at the septum and the base, and at the base
173 alone in division intermediates (Supp. Fig. S4B).

174 **MreB Filament Formation is not Required for Foci Formation by FtsK, PBP2, and PBP3**

175 MreB was one of the last components that associated with nascent divisomes forming at the
176 base of the progenitor mother cell (Fig. 2C). To investigate whether MreB filament formation

177 was required for the formation of foci by the other chlamydial divisome components, HeLa cells
178 were infected with *Ct* transformed with the FtsK, PBP2, PBP3, MreC, or MreB fusions, and the
179 fusions were induced by adding 10nM aTc to the media of the infected cells at 20hpi for 1hr.
180 During the induction period, cells were incubated in the absence (Figs. 3B and 3D) or presence
181 (Figs. 3C and 3E) of the MreB inhibitor, A22, which inhibits MreB filament formation (Bean,
182 2009). RBs were harvested at 21hpi and stained with the appropriate antibodies to assess the
183 effect of A22 on the cellular distribution of the fusions. As previously shown (Ouellette SP 2012;
184 Cox 2020), A22 inhibits chlamydial budding and most cells in the population were coccoid
185 following A22 treatment (Fig. 3A). Furthermore, approximately 50% of the untreated control
186 cells were coccoid, which is consistent with prior estimates of the number of non-dividing RBs at
187 this stage of the developmental cycle (Lee 2018), indicating that our lysis procedure does not
188 lead to a bias in the number of non-dividing coccoid cells in the population. MreB in coccoid
189 cells adopted a diffuse pattern of localization following A22 treatment (Fig 3). A22 also had a
190 statistically significant effect on the percent of coccoid cells containing MreC foci, but it did not
191 affect the ability of FtsK, PBP2, or PBP3 to form foci in coccoid cells (Figs. 3D and 3E). These
192 data indicate that MreB filaments do not function as a scaffold that is necessary for the assembly
193 of all divisome components in *Ct*.

194 **Effect of *ftsk* and *pbp2* Knockdown on Cell Division and Divisome Assembly in *Ct***

195 To further investigate the mechanisms that regulate divisome assembly in *Ct*, we inducibly
196 repressed the expression of *ftsK* or *pbp2* using CRISPRi technology, which has been used to
197 inducibly repress the expression of genes in *Ct* (Ouellette SP 2021). CRISPRi employs a
198 constitutively expressed crRNA that targets an inducible dCas enzyme (dCas12) to specific
199 genes where it binds but fails to cut, thus inhibiting transcription. We transformed *Ct* with the

200 pBOMBL12CRia plasmid that constitutively expresses an *ftsK* or *pbp2*-specific crRNA, which
201 target sequences in the *ftsK* or *pbp2* promoter regions. To determine whether *ftsK* and *pbp2*
202 transcript levels were altered using this CRISPRi approach, dCas12 expression was induced by
203 the addition of 5nM aTc to the media of infected cells at 8hpi. Control cells were not induced.
204 Nucleic acids were isolated from induced cells and uninduced control cells at various times, and
205 RT-qPCR was used to measure *ftsK* or *pbp2* transcript levels. This analysis revealed that the
206 induction of dCas12 resulted in ~10-fold reduction in *ftsK* transcript levels by 15hpi in cells
207 expressing the *ftsK*-targeting crRNA (Supp. Fig. S5A), and ~8-fold reduction in *pbp2* transcript
208 levels in cells expressing the *pbp2*-targeting crRNA (Supp. Fig. S5B), while these crRNAs had
209 minimal or no effect on chlamydial *euo* and *omcB* transcript levels, suggesting that the *ftsK* and
210 *pbp2* crRNAs specifically inhibit the transcription of *ftsK* and *pbp2* (Supp. Figs. S5A and S5B).
211 To investigate the effect of *ftsK* or *pbp2* down-regulation on developmental cycle progression,
212 dCas12 was induced by the addition of aTc to the media of infected cells at 4hpi. Control cells
213 were not induced. The cells were then fixed at 24hpi and stained with MOMP and Cas12
214 antibodies. Imaging analysis revealed that *Ct* morphology was normal and dCas12 was
215 undetectable in the inclusions of uninduced control cells, while foci of dCas12 were observed in
216 the induced cells, and *Ct* in the inclusion exhibited an enlarged aberrant morphology (Supp. Figs.
217 S5C and S5D), suggesting that the inducible knockdown of *ftsK* or *pbp2* blocks chlamydial cell
218 division. In additional studies, we induced dCas12 at 17hpi in cells expressing the *ftsK* or *pbp2*-
219 targeting crRNAs. Lysates were prepared and the cells were fixed at 21hpi, and localization
220 studies revealed that foci of endogenous FtsK and PBP2 were almost undetectable when *ftsK* or
221 *pbp2* were transiently knocked down using this CRISPRi approach (Supp. Fig. S5E).

222 To assess whether the knockdown of *ftsK* or *pbp2* arrests *Ct* division at a specific stage of
223 polarized budding, HeLa cells were infected with *Ct* transformed with the pBOMBL12CRia
224 plasmids encoding the *ftsK* or *pbp2*-targeting crRNAs. At 17hpi, dCas12 was induced by the
225 addition of 20nM aTc to the media. Control cells were not induced. RBs were harvested from
226 induced and uninduced control cells at 22hpi and stained with MOMP antibodies, and imaging
227 analyses quantified the division intermediates present in the population. These analyses revealed
228 that >60% of the *Ct* in the uninduced controls were at various stages of polarized budding (Figs.
229 4A and B), while ~90% of the cells were coccoid when *ftsK* was knocked down (Fig. 4A), and
230 ~85% of the cells were coccoid following *pbp2* knockdown (Fig. 4B), suggesting that the
231 initiation of polarized budding of *Ct* is inhibited when *ftsK* or *pbp2* are knocked down.
232 We next examined whether the knockdown of *ftsK* affected foci formation by PBP2 or PBP3
233 in coccoid cells. HeLa cells were infected with *Ct* transformed with the pBOMBL12CRia
234 plasmid encoding the *ftsK*-targeting crRNA. At 17hpi, dCas12 was induced by the addition of
235 10nM aTc to the media. Control cells were not induced. RBs were harvested from induced and
236 uninduced control cells at 22hpi, and the localization of endogenous PBP2 and PBP3 in coccoid
237 cells was assessed (Figs. 4C and 4D). This analysis revealed that the number of coccoid cells
238 with polarized foci of PBP2 and PBP3 were reduced by approximately 80% following *ftsK*
239 knockdown (Fig. 4E). In similar analyses, we assessed the effect of *pbp2* knockdown on the
240 ability of FtsK and PBP3 to form foci in coccoid cells. While FtsK retained its ability to form
241 foci in coccoid cells following *pbp2* knockdown, foci of PBP3 were almost entirely absent in
242 *pbp2* knockdown cells (Figs. 4C and 4D). Quantification of these assays revealed that FtsK is
243 necessary for foci formation by both the PBP2 and PBP3 transpeptidases, while PBP2 is
244 necessary for foci formation by PBP3 (Figs. 4E and 4F). Our data place FtsK upstream of, and

245 necessary for, the addition of PBP2 and PBP3 to the *Ct* divisome, and PBP2 upstream of and
246 necessary for the addition of PBP3 to the *Ct* divisome. These results are consistent with inhibitor
247 studies that indicated PBP2 acts upstream of PBP3 in the polarized budding process of *Ct* (Cox
248 2020).

249 To investigate whether the catalytic activity of PBP2 is necessary to maintain its association
250 with the *Ct* divisome, HeLa cells were infected with *Ct*, and mecillinam, an inhibitor of the
251 transpeptidase activity of PBP2 (Kocaoglu 2015; Cox 2020), was added to the media of infected
252 cells at 20hpi. Cells incubated in the absence of mecillinam were included as a control.
253 Mecillinam-treated and control cells were harvested at 22hpi and the effect of inhibiting the
254 catalytic activity of PBP2 on the localization of FtsK, PBP2, and PBP3 was determined. As
255 shown previously, mecillinam blocks chlamydial division (Ouellette SP 2012; Cox 2020), and
256 most cells in the population assumed a coccoid morphology (Fig. 5A). We then determined the
257 localization of endogenous FtsK, PBP2, and PBP3 in drug-treated and control coccoid cells.
258 Mecillinam treatment resulted in a ~50% reduction in the number of cells with polarized foci of
259 PBP2 (Figs. 5B - 5E). There was a similar reduction in polarized foci of PBP3 following
260 mecillinam treatment (Figs. 5B - 5E). These data indicate that the catalytic activity of PBP2 is
261 necessary for PBP2 to efficiently associate with or maintain its association with polarized
262 divisome complexes. Furthermore, consistent with *pbp2* knockdown studies, PBP3 association
263 with the divisome complex is dependent on the prior addition of PBP2 to the complex, but foci
264 formation by FtsK is unaffected when PBP2 foci are reduced in number (Fig. 5).

265 **Effect of Inhibitors and *ftsk* Knockdown on PG Organization in *Ct***

266 To assess the morphology of PG at the septum and the base of dividing cells, we used an
267 EDA-DA labeling strategy (Liechti 2014; Cox 2020). This approach enabled the detection of PG

268 foci, bars, and rings in dividing *Ct* (Liechti 2021). Our imaging analysis revealed that in some
269 instances PG foci were detected at both the septum and at the base of the progenitor mother cell
270 (Fig. 6A), and in other instances PG organization at the septum and the base differed. In the
271 example shown (Fig. 6B), a PG foci was detected at the septum while a PG ring was detected at
272 the base of the mother cell. In additional analyses, we compared the localization of mCherry-
273 PBP3 to the localization of PG in cells where the expression of this mCherry fusion had been
274 induced by the addition of aTc to the media. This analysis, which was restricted to PG formation
275 at the septum of dividing cells, revealed that multiple foci of PBP3 were associated with a septal
276 PG ring (Fig. 6C). Furthermore, the PG ring was at an angle relative to the MOMP-stained
277 septum. Similar analyses revealed that 2 foci of endogenous FtsK were associated with PG that
278 was again at an angle relative to the MOMP-stained septum. This was true even though the PG
279 had not fully reorganized into a ring structure (Fig. 6C).
280 We then determined the effect of A22 and mecillinam on PG synthesis/organization. Since
281 both of these drugs induce *Ct* to assume a coccoid morphology, we initially characterized PG
282 organization in untreated coccoid cells. We detected foci, bars, or rings in ~80% of untreated
283 coccoid cells (Figs. 6D and 6E), which make up ~50% of the cells in the inclusion at this stage of
284 the developmental cycle (Lee 2018). Furthermore, each of these PG intermediates exhibited a
285 polarized distribution in untreated coccoid cells (Fig. 6D). Although we cannot rule out that
286 continued PG synthesis and reorganization occurs in polarized division intermediates, PG rings
287 can arise prior to any of the morphological changes that occur during the polarized division of
288 *Ct.*
289 Prior studies have shown that inhibitors of MreB filament formation prevent the appearance
290 of PG-containing structures in *Ct* (Liechti 2014; Ouellette SP 2022). To assess whether MreB

291 filament formation is required for PG synthesis and/or PG reorganization, we infected HeLa cells
292 with *Ct*, and EDA-DA and A22 were added to the media of infected cells at 18hpi. The cells
293 were harvested at 22hpi, lysates were prepared, and PG localization was determined. These
294 analyses revealed that PG was diffuse/undetectable in the majority of A22-treated cells, and, in
295 those cells where PG was still detected, it could not convert into ring structures (Figs. 6E and
296 6F). In similar experiments, we assessed the effect of mecillinam on the appearance of PG
297 intermediates in coccoid cells. These analyses revealed that PG formed discrete foci or bars in
298 60% of mecillinam-treated cells (Figs. 6E and 6F). However, these PG intermediates could not
299 convert into PG rings when the transpeptidase activity of PBP2 was inhibited. Finally, we
300 assessed PG organization in cells where *ftsK* was knocked down by inducing dCas12 in the *ftsK*
301 knockdown strain by the addition of aTc to the media of infected cells at 17hpi. Cells were fixed
302 at 21hpi, and localization studies revealed that *ftsK* knockdown had the most dramatic effect on
303 PG localization, which was diffuse/undetectable in ~90% of the cells assayed. Inhibiting
304 divisome assembly by knocking down *ftsK* almost entirely prevented the accumulation of all PG-
305 containing intermediates in *Ct* (Figs. 6E and 6F).

---

306 **Discussion**

307 The results presented here provide insight into the molecular mechanisms governing the
308 FtsZ-less polarized cell division process of *Ct*. This study is the first to document the ordered
309 assembly of divisome proteins in *Ct* and to investigate the roles of divisome proteins in
310 regulating PG synthesis/organization in this obligate intracellular bacterial pathogen. Our studies
311 showed that the divisome in *Ct* is hybrid in composition, containing elements of the divisome
312 and elongasome from other bacteria, and a putative pathway for the assembly of the novel hybrid
313 divisome of *Ct* is shown in Fig. 6G. Although we focused our study on a subset of the divisome
314 and elongasome proteins that *Chlamydia* expresses (bolded in Fig. 6G), our results support our
315 conclusion that chlamydial budding is dependent upon a hybrid divisome complex and that FtsK
316 is required for the assembly of this hybrid divisome. At this time, we cannot rule out that other
317 proteins act upstream of FtsK to initiate divisome assembly in this obligate intracellular bacterial
318 pathogen.

319 The domain organization of FtsK is highly conserved among bacteria. The C-terminus of the
320 protein mediates the ATP-dependent directional translocation of the protein along DNA through
321 interaction with KOPS (Fts**K** **o**rienting **p**olar **s**equences) (Barre, 2001; Massey, 2006) and stimulates
322 XerCD-dependent recombination at the *dif* site near the chromosomal terminus to decatenate
323 chromosomal dimers that arise from homologous recombination during DNA replication to monomers
324 (Blakely, 1993; Massey, 2006). The C-terminus of chlamydial FtsK is 41% identical to the C-terminus of
325 *E. coli* FtsK. The N-terminus of *E. coli* FtsK encodes 4 predicted transmembrane spanning helices, which
326 are sufficient to direct the protein to the septum in dividing cells (Yu, 1998). The N-terminus of
327 chlamydial FtsK, which is also predicted to encode 4 transmembrane-spanning helices, is 34% identical to
328 *E. coli* FtsK.

329 Our analyses revealed a novel spatiotemporal localization pattern of FtsK during the
330 chlamydial division process. Chlamydial FtsK forms discrete foci at the septum, foci at the
331 septum and at the base of the mother cell, or in foci only at the base of the mother cell (Figure 1).
332 Our data indicate that the foci at the base of the mother cell correspond to nascent divisome
333 complexes that form prior to the formation of a secondary bud at the base of the progenitor
334 mother cell. Our analyses further revealed there was no correlation between the stage of bud
335 formation by the initial bud (early, mid-late; Ouellette SP, 2022), and the appearance of nascent
336 divisomes at the base of the progenitor mother cell (data not shown).
337 The *Ct* divisome is hybrid in nature, containing elements of the divisome (FtsK and PBP3)
338 and elongasome (PBP2, MreB, and MreC) from other bacteria. Each of these proteins formed
339 foci at the septum, foci at the septum and at the base of the mother cell, or foci only at the base of
340 the mother cell, and the foci of each protein were restricted to one side of the MOMP-stained
341 septum (Figs. 1 and 2). Knockdown of *ftsK* using CRISPRi revealed that FtsK is necessary for
342 the assembly of this hybrid divisome complex (Fig. 4). Knockdown and inhibitor studies further
343 revealed that PBP2 is necessary for the addition of PBP3 to the divisome in *Ct* (Figs. 4 and 5).
344 The chlamydial divisome proteins all form foci in coccoid cells (Figs. 1 and 2), and FtsK
345 forms foci in dividing *Ct* that only partially overlap the distribution of PBP2, PBP3, MreC, and
346 MreB (Fig. 2 and Supp. Fig. S4A). The lack of overlap of FtsK with MreB and MreC is most
347 clearly evident in Supp. Fig. S4A, and while it is unclear why FtsK only partially overlaps the
348 distribution of the other divisome components in dividing *Ct*, MreB (Liechti 2014; Kemege
349 2015; Lee 2020) and MreC (Supp. Fig. S6A) can reorganize into rings in dividing cells, and the
350 MreC rings we detected, like PG rings (Fig. 6), were at an angle relative to the MOMP-stained
351 septum. MreC also forms rings in coccoid cells (Supp. Fig. S6B). Although MreB and MreC

352 form rings in *Ct*, we never detected FtsK rings in dividing or coccoid chlamydial cells. The
353 relevance of the angled orientation of PG and MreC rings relative to the MOMP-stained septum
354 in division intermediates is unclear. However, it appears to be a conserved feature of the cell
355 division process and may arise because the divisome proteins are often positioned slightly above
356 or below the plane of the MOMP-stained septum (Figs. 1 and 2).

357 Previous studies hypothesized that MreB filaments may substitute for FtsZ and form a
358 scaffold necessary for the assembly of the divisome in *Ct* (Ouellette SP 2012; Ouellette SP 2015;
359 Ouellette SP 2020). However, our analyses have indicated that MreB is one of the last
360 components recruited to nascent divisomes that form at the base of the mother cell in *Ct,* and
361 localization studies revealed that foci formation by FtsK, PBP2, and PBP3 are not dependent on
362 MreB filament formation (Fig. 3). Although our data indicate that MreB filaments do not form a
363 scaffold necessary for the assembly of all components of the divisome in *Ct*, MreB filaments are
364 necessary for the conversion of PG foci into PG rings in *Ct* (Fig. 6).

365 FtsZ treadmilling drives its rotational movement at the septum and this may be required for
366 the positioning of peptidoglycan biosynthetic enzymes at the division plane in gram-negative and
367 gram-positive bacteria (Bisson-Filho 2017; Yang 2017). The knockdown studies presented here
368 demonstrated that in the absence of FtsZ, chlamydial FtsK is critical for divisome assembly and
369 PG synthesis in *Ct,* and future real-time imaging studies will determine whether changes in the
370 organization/distribution of FtsK occur during chromosomal translocation and/or cell division in
371 *Chlamydia*. Furthermore, future studies will investigate the mechanisms that regulate the site of
372 assembly of nascent divisomes in the mother cell during the polarized cell division process.

373 *Ct* is a member of the Planctomycetes/Verrucomicrobia/Chlamydia superphylum and
374 members of the Chlamydia and Planctomycetes phyla do not encode FtsZ (Rivas-Marín 2016).

375 *Planctospirus limnophila* is a member of the Planctomycetes that divides by polarized budding,
376 and recent knockout studies (Rivas-Marin 2023) indicated that FtsK is the only protein of the
377 chlamydial divisome we characterized here that is essential for the growth of this free-living
378 organism. These results suggest that multiple mechanisms of FtsZ-independent polarized
379 budding have evolved in members of this superphyla. It will be of interest in future studies to
380 determine whether other members of the Planctomycetes that bud (Wiegand 2020) divide using a
381 divisome apparatus similar to *Ct*.

382 **Materials and Methods**

383 **Cell Culture**

384 HeLa cells (ATCC, Manassas, VA) were cultured in Dulbecco's Modified Eagle Medium
385 (DMEM; Invitrogen, Waltham, MA) containing 10% fetal bovine serum (FBS, Hyclone, Logan,
386 UT) at 37°C in a humidified chamber with 5% CO2. HeLa cells were infected with *Ct* serovar L2
387 434/Bu in the same media. Infections of HeLa cells with chlamydial transformants were
388 performed in DMEM containing 10% FBS and 0.36 U/mL penicillin G (Sigma-Aldrich).

389 **Cloning**

390 The plasmids and primers used for generating mCherry fusions of FtsK, PBP2, PBP3,
391 and MreC are listed in Supp. Table S1. The chlamydial *ftsK*, *pbp2, pbp3,* and *mreC* genes were
392 amplified by PCR with Phusion DNA polymerase (NEB, Ipswich, MA) using 10
393 ng *C. trachomatis* serovar L2 genomic DNA as a template. The PCR products were purified
394 using a PCR purification kit (Qiagen) and inserted into the pBOMB4-Tet (-GFP) plasmid, which
395 confers resistance to β-lactam antibiotics. The plasmid was cut at the NotI (FtsK-mCherry) or the
396 KpnI (mCherry-PBP2, mCherry-PBP3, mCherry-MreC) site, and the chlamydial genes were
397 inserted into the cut plasmid using the HiFi DNA Assembly kit (NEB) according to the

398 manufacturer's instructions. The products of the HiFi reaction were transformed into NEB-
399 5αI^{q} competent cells (NEB) and transformants were selected by growth on plates containing
400 ampicillin. DNA from individual colonies was isolated using a mini-prep DNA isolation kit
401 (Qiagen), and plasmids were initially characterized by restriction digestion to verify the inserts
402 were the correct size. Clones containing inserts of the correct size were DNA sequenced prior to
403 use.

404 **DNA and RNA purification and RT-qPCR**

405 Total nucleic acids were extracted from HeLa cells infected with *Ct* plated in 6-well dishes as
406 described previously (Ouellette 2015, Ouellette, Blay et al. 2021). For RNA isolation, cells were
407 rinsed one time with PBS, then lysed with 1mL Trizol (Invitrogen) per well. Total RNA was
408 extracted from the aqueous layer after mixing with 200µL per sample of chloroform following
409 the manufacturer's instructions. Total RNA was precipitated with isopropanol and treated with
410 DNase (Ambion) according to the manufacturer's guidelines prior to cDNA synthesis using
411 SuperScript III (Invitrogen). For DNA, infected cells were rinsed one time with PBS, trypsinized
412 and pelleted before resuspending each pellet in 500µL of PBS. Each sample was split in half, and
413 genomic DNA was isolated from each duplicate sample using the DNeasy extraction kit
414 (Qiagen) according to the manufacturer's guidelines. Quantitative PCR was used to measure
415 *C. trachomatis* genomic DNA (gDNA) levels using an *euo* primer set. 150ng of each sample was
416 used in 25µL reactions using standard amplification cycles on a QuantStudio3 thermal cycler
417 (Applied Biosystems) followed by a melting curve analysis. *ftsK, pbp2, euo*, and *omcB* transcript
418 levels were determined by RT-qPCR using SYBR Green as described previously (Ouellette SP
419 2021) (see Supp. Table S2 for primers used for measuring gDNA levels and RT-qPCR).
420 Transcript levels were normalized to genomes and expressed as ng cDNA/gDNA.

421 **Transformation of *Ct***

422 *Ct* was transformed as described previously (Wang 2011). Briefly, HeLa cells were plated in
423 a 10cm plate at a density of 5 x 10^6 cells the day before beginning the transformation
424 procedure. *Ct* lacking its endogenous plasmid (-pL2) was incubated with 10µg of plasmid DNA
425 in Tris-$CaCl_2$ buffer (10 mM Tris-Cl pH 7.5, 50 mM $CaCl_2$) for 30 min at room temperature.
426 HeLa cells were trypsinized, washed with 8mL of 1x DPBS (Gibco), and pelleted. The pellet was
427 resuspended in 300µL of the Tris-$CaCl_2$ buffer. *Ct* was mixed with the HeLa cells and incubated
428 at room temperature for an additional 20 min. The mixture was added to 10mL of DMEM
429 containing 10% FBS and 10 µg/mL gentamicin and transferred to a 10cm plate. At 48hpi, the
430 HeLa cells were harvested and *Ct* in the population were used to infect a new HeLa cell
431 monolayer in media containing 0.36 U/ml of penicillin G to select for transformants. The plate
432 was incubated at 37°C for 48 hours. These harvest and re-infection steps were repeated every
433 48hrs until inclusions were observed.

434 **Immunofluorescence Microscopy**

435 HeLa cells were seeded in 10cm plates at a density of 5 x 10^6 cells per well the day before the
436 infection. *Ct* L2 or chlamydial strains transformed with plasmids encoding FtsK-mCherry,
437 mCherry-PBP2, mCherry-PBP3, or mCherry-MreC or with plasmids that direct the constitutive
438 expression of the crRNAs targeting the *pbp2* or *ftsK* promoters were used to infect HeLa cells in
439 DMEM. For experiments with the transformants, aTc was added to the media of infected cells at
440 the indicated concentration and time. At 21hpi, cells were detached from the 10cm plate by
441 scraping and pelleted by centrifugation for 30 seconds. The pellet was resuspended in 1 mL of
442 0.1x PBS (Gibco) and transferred to a 2mL tube containing 0.5mm glass beads (ThermoFisher
443 Scientific). Cells were vortexed for 3 mins. then centrifuged at 800rpm for 2 mins. in a

444 microfuge. 20μLs of the supernatant was mixed with 20μLs of 2x fixing solution (6.4%
445 formaldehyde and 0.044% glutaraldehyde) and incubated on a glass slide for 10 min at room
446 temperature. Cells were washed with 3 times with PBS, and the cells were permeabilized by
447 incubation with PBS containing 0.1% Triton X-100 for 1 min. Cells were washed with PBS two
448 times. For experiments with *Ct* L2, the cells were incubated with a goat primary antibody against
449 the major outer-membrane protein (MOMP; Meridian, Memphis, TN), and the mouse primary
450 antibody that recognizes endogenous FtsK raised against recombinant CT739 protein
451 (**https://doi.org/10.1099/mic.0.047746-0**), or with rabbit antibodies raised against peptides
452 derived from PBP 2 or PBP3 (Ouellette SP 2012) . Briefly, chlamydial antigens or peptides
453 emulsified with Freund's incomplete adjuvant were used to immunize animals via intramuscular
454 injections three times with an interval of 2 weeks. Antisera were collected from the immunized
455 animals 2 to 4 weeks after the final immunization as the primary antibodies. After the primary
456 antibody labeling, the cells were then rinsed with PBS and incubated with donkey anti-goat IgG
457 (Alexa 488) and donkey anti-mouse IgG (Alexa 594) or donkey-anti-rabbit IgG (Alexa 594)
458 secondary antibodies (Invitrogen). Experiments in which we visualized the distribution of the
459 various mCherry fusions, the localization of the mCherry fluorescence was compared to the
460 distribution of MOMP. In some experiments, we determined the distribution of the MreB_6x His
461 fusion by staining cells expressing the fusion with a rabbit anti-6x His antibody (Abcam,
462 Cambridge, MA) and the goat anti-MOMP antibody followed by the appropriate secondary
463 antibodies. Cells were imaged using Zeiss AxioImager2 microscope equipped with a 100x oil
464 immersion PlanApochromat objective and a CCD camera. During image acquisition, 0.3μm xy-
465 slices were collected that extended above and below the cell. The images were collected such
466 that the brightest spot in the image was saturated. The images were deconvolved using the

467 nearest neighbor algorithm in the Zeiss Axiovision 4.7 software. Deconvolved images were
468 viewed and assembled using Zeiss Zen-Blue software. For each experiment, three independent
469 replicates were performed, and the values shown for localization are the average of the 3
470 experiments. In some instances, 3D projections of the acquired xy slices were generated using
471 the Zeiss Zen-Blue software.

472 **Peptidoglycan (PG) labeling**

473 PG was labeled by incubating cells with 4mM ethylene-D-alanine-D-alanine (E-DA-DA) as
474 described (Cox 2020). The incorporated E-DA-DA was fluorescently labeled using the Click &
475 Go™ labeling kit (Vector Laboratories). The distribution of fluorescently labeled PG was
476 compared to the distribution of MOMP and endogenous FtsK or the distribution of mCherry-
477 PBP3. Three independent replicates were performed, and the values shown are the average of the
478 3 experiments.

479 **Inclusion forming unit assay**

480 HeLa cells were infected with *Ct* (-pL2) transformed with the pBOMB4 Tet (-GFP) plasmid
481 encoding the indicated aTc-inducible gene. At 8hpi, aTc was added to the culture media at the
482 indicated concentration. Control cells were not induced. At 48hpi, the HeLa cells were dislodged
483 from the culture dishes by scraping and collected by centrifugation. The pellet was resuspended
484 in 1 mL of 0.1x PBS (Gibco) and transferred to a 2mL tube containing 0.5mm glass bead tubes
485 (ThermoFisher Scientific). Cells were vortexed for 3 min. followed by centrifugation at 800rpm
486 for 2 min. The supernatants were mixed with an equal volume of a 2x sucrose-phosphate (2SP)
487 solution (ref) and frozen at -80°C. At the time of the secondary infection, the chlamydiae were
488 thawed on ice and vortexed. Cell debris was pelleted by centrifugation for 5 min at 1k x g at 4°C.
489 The EBs in the resulting supernatant were serially diluted and used to infect a monolayer of

490 HeLa cells in a 24-well plate. The secondary infections were allowed to grow at 37°C for 24 hrs
491 before they were fixed and labeled for immunofluorescence microscopy by incubating with a
492 goat anti-MOMP antibody followed by a secondary donkey anti-goat antibody (Alexa Fluor
493 594). The cells were rinsed in PBS and inclusions were imaged using an EVOS imaging system
494 (Invitrogen). The number of inclusions were counted in 5 fields of view and averaged. Three
495 independent replicates were performed, and the values from the replicates were averaged to
496 determine the number of inclusion forming units. Chi-squared analysis was used to compare
497 IFUs in induced and uninduced samples.

498 **Effect of A22 and mecillinam on the profile of division intermediates and on PG and**
499 **divisome protein localization in *Ct***

500 HeLa cells were infected with *Ct* transformed with the pBOMB4-Tet (-GFP) plasmid
501 encoding FtsK-mCherry, mCherry-PBP2, mCherry-PBP3, mCherry-MreC, or MreB-6xHis. The
502 fusions were induced at 20hpi with 10nM aTc for 1hr in the absence or presence of 75 μM A22.
503 At 22hpi, cells were harvested and prepared for staining as described above. Three independent
504 replicates were performed, and the values shown for localization are the average of the 3
505 experiments.

506 HeLa cells were infected with *Ct* L2 and 20μM mecillinam (Sigma) was added to the media
507 of infected cells at 17 hpi. Control cells were untreated. At 22 hpi, infected cells were harvested
508 and RBs were prepared and stained with MOMP, FtsK, PBP2 or PBP3 antibodies as described
509 above. Alternatively, cells were incubated with 4mM EDA-DA at 17hpi in the presence or
510 absence of 20μM mecillinam. The cells were harvested at 22hpi, and RBs were prepared and PG
511 was click-labeled, and its distribution was visualized in MOMP-stained cells as described above.

512 Three independent replicates were performed, and the values shown for localization are the
513 average of the 3 experiments.

514 **Immunoblotting**

515 HeLa cells infected with *Ct* L2 were harvested by scraping the infected cells from the plate at
516 24hpi. Uninfected HeLa cells were included as a control. The HeLa cells were pelleted by
517 centrifugation, resuspended in SDS sample buffer and electrophoresed on a 10% SDS
518 polyacrylamide gel. The gel was electrophoretically transferred to nitrocellulose (Schleicher and
519 Schuell), and the filter was incubated with mouse polyclonal antibodies raised against
520 chlamydial FtsK. The filter was rinsed and incubated with 800 donkey anti-mouse IgG secondary
521 antibodies (LICOR, Lincoln, NE) and imaged using a LICOR Odyssey imaging system.
522 HeLa cells were infected with *Ct* transformed with plasmids that inducibly express FtsK-
523 mCherry, mCherry-PBP2, mCherry-PBP3, or mCherry-MreC. The fusions were induced by the
524 addition of 10nM aTc to the media of infected cells at 17hpi. The cells were harvested and
525 pelleted at 21hpi. The cell pellet was resuspended in 1 mL of 0.1x PBS (Gibco) and transferred
526 to a 2mL tube containing 0.5mm glass beads (ThermoFisher Scientific). Cells were vortexed for
527 3 min. followed by centrifugation at 800rpm for 2 min. The supernatant was collected and
528 centrifuged for 3 min at 13,000 rpm and the pellet containing *Ct* was resuspended in TBS
529 containing 1% TX-100, 1X protease inhibitor cocktail (Sigma), and 5μM lactacystin. The
530 suspension was sonicated 3 times on ice and centrifuged at 13,000 rpm for 3 mins. The
531 supernatant was collected and mixed with SDS sample buffer. The samples were boiled and
532 electrophoresed on a 10% SDS polyacrylamide gel, and the gel was electrophoretically
533 transferred to nitrocellulose. The blots from these analyses were probed with a rabbit anti-

534 mCherry primary antibody (Invitrogen) and a 800 donkey anti-rabbit IgG secondary antibodies
535 (LICOR, Lincoln, NE). The filters were imaged using a LICOR Odyssey imaging system.
536 HeLa cells were infected with *Ct* transformed with the pBOMB4-Tet (-GFP) plasmid
537 encoding mCherry-PBP2 or mCherry-PBP3. The fusions were induced with 10nM aTc at 17hpi.
538 Uninduced cells were included as a control. The cells were harvested at 21hpi, and samples were
539 processed for immunoblotting as described above. The blots were probed with rabbit polyclonal
540 antibodies raised against peptides derived from chlamydial PBP2 or PBP3 (Ouellette SP 2012).
541 The blots were then rinsed and incubated with 800 donkey anti-rabbit IgG secondary antibodies
542 (LICOR, Lincoln, NE). The filters were imaged using a LICOR Odyssey imaging system.

543 **ACKNOWLEDGMENTS**

544 We thank Dr. H. Caldwell (NIH/NIAID) for providing eukaryotic cell lines and Dr. I. Clarke
545 (University of Southampton) for providing the plasmidless strain of *C. trachomatis* serovar L2.
546 Funding for this work was supported in part by the National Institutes of Health (NIH/NIGMS)
547 grant R35GM151971 to SPO and by the NSF grant 1817578 to JVC.

548

549 **Figure Legends**

550 **Figure 1:**(A) The linear divisome assembly pathway of *E. coli* is shown. *Ct* encodes the
551 divisome proteins boxed in red. HeLa cells were infected with *Ct* L2 and RBs were prepared at
552 21hpi. The cells were fixed and stained with MOMP (green) and FtsK (red) antibodies. The
553 distribution of FtsK in (B) coccoid cells and in (C) cell division intermediates that had not
554 initiated secondary bud formation is shown. Bars are 1 μm. HeLa cells were infected with *Ct*
555 transformed with the pBOMB4 -Tet (-GFP) plasmid encoding FtsK-mCherry. The fusion was
556 induced with 10nM aTc for 1 hr. and RBs were prepared from infected HeLa cells at 21hpi and

557 stained with MOMP antibodies (green). The distribution of MOMP relative to the mCherry
558 fluorescence (D) in coccoid cells and in (E) cell division intermediates that had not initiated
559 secondary bud formation is shown. Bars are 1μm. Arrowheads in C and E denote foci of FtsK
560 above or below the MOMP-stained septum. (F) HeLa cells were infected with *Ct* L2. At 21hpi,
561 the cells were harvested and RBs were stained with MOMP antibodies. The number of dividing
562 cells that had initiated secondary bud formation was quantified in 150 cells. Three independent
563 replicates were performed, and the values shown are the average of the 3 replicates. (G)
564 Endogenous FtsK and FtsK-mCherry accumulate in foci at the septum of secondary buds
565 (marked with arrowheads).
566 **Figure 2:** HeLa cells were infected with *Ct* transformed with PBP2, PBP3, or MreC with an N-
567 terminal mCherry tag, or with *Ct* transformed with an MreB_6xHis fusion (Lee 2020). Each of
568 the fusions was induced by adding 10nM aTc to the media at 17hpi. Lysates were prepared at
569 21hpi and the cells were fixed and stained with a MOMP antibody. The distribution of the
570 mCherry fluorescence in (A) coccoid cells and in (B) dividing cells that had not initiated
571 secondary bud formation is shown. Cells expressing the MreB_6xHis fusion were stained with
572 rabbit anti-6x His antibody (red) and MOMP antibodies (green). Dividing cells with foci at the
573 septum, foci at the septum and foci at the base of the mother cell, or foci at the base alone are
574 shown for each of the fusions. Arrowheads in B denote foci of the divisome proteins above or
575 below the plane of the MOMP-stained septum. (C) HeLa cells were infected with *Ct* L2.
576 Alternatively, cells were infected with *Ct* that were transformed with FtsK-mCherry, mCherry-
577 PBP2, mCherry-PBP3, mCherry-MreC, or MreB_6xHis. The cells expressing the fusions were
578 induced with aTc for 1.5hrs then fixed at 21hpi and the distribution of endogenous FtsK, or the
579 mCherry fluorescence in cells inducibly expressing the mCherry fusions, or the distribution of

580 MreB in cells where the MreB_6xHis fusion was inducibly expressed was quantified. A small
581 fraction (2 %) of dividing cells contained multiple foci of each of the divisome proteins at the
582 septum and/or the base of the cell. Since these cells were relatively rare, we included these cells
583 with cells that contained a single foci in the quantification. The localization profiles were
584 quantified in 100 cells. Three independent replicates were performed, and the values shown are
585 the average of the 3 replicates. Chi-squared analysis revealed that the localization profiles of
586 endogenous FtsK and FtsK-mCherry are not statistically different from each other, but they are
587 statistically different than the PBP2, PBP3, MreC and MreB localization profiles (* – $p<0.009$).
588 The localization profile of the MreB fusion is also statistically different than the localization
589 profiles of the mCherry fusions of PBP2 and PBP3 (#- $p = 0.05$). (D) Hela cells were infected
590 with *Ct* transformed with PBP2, PBP3, or MreC with a N-terminal mCherry tag, or with *Ct*
591 transformed with an MreB_6xHis fusion (Lee 2020). The fusions were induced by adding 10 nM
592 aTc to the media at 17hpi. The cells were harvested at 21hpi and *Ct* were harvested and stained
593 with FtsK and MOMP antibodies. The cells expressing the MreB fusion were stained with FtsK,
594 MOMP, and 6xHis antibodies. Imaging analyses revealed that FtsK was present in foci at the
595 septum and in foci at the base in these cells, while each of the fusions was only detected at the
596 septum where they overlapped the distribution of septal FtsK (Bars are1μm).
597 **Figure 3:** (A) HeLa cells infected with *Ct* L2 were treated with 75μM A22 for 1 hour. Control
598 cells were not treated with A22. Lysates were prepared at 21hpi and the number of coccoid and
599 dividing cells in the population were quantified in 100 cells. Three independent replicates were
600 performed, and the values shown are the average of the 3 replicates. (B-E) Alternatively, HeLa
601 cells were infected with *Ct* transformed with plasmids encoding FtsK-mCherry, mCherry-PBP2,
602 mCherry-PBP3, mCherry-MreC, or MreB-6xHis. The fusions were induced at 20hpi with 10nM

603 aTc for 1hr in the absence (B and D) or presence (C and E) of 75μM A22. Coccoid cells
604 prepared from the infected cells at 21hpi were stained with MOMP antibodies (green). The
605 MreB-6xHis fusion was also stained with 6xHis antibodies (red). Panel B shows the distribution
606 of the fusions in untreated coccoid cells. Panel C illustrates the effect of A22 on the localization
607 of the fusions in coccoid cells. Bars in B and C are 1μm. The distribution of FtsK-mCherry,
608 mCherry-PBP2, mCherry-PBP3, mCherry-MreC, and MreB-6xHis was quantified in (D) control
609 coccoid cells and in (E) A22-treated cells coccoid cells (n=50) is shown. Three replicates were
610 performed, and the values shown in D and E are the averages of the 3 replicates. Student T-test
611 indicated that A22 had a statistically significant effect on the localization of MreB and MreC (* –
612 $p<0.01$).

613 **Figure 4:** HeLa cells were infected with *Ct* transformed with the pBOMBL-12CRia plasmid,
614 which constitutively expresses a *ftsK* crRNA or *pbp2* crRNA and encodes dCas12 under the
615 control of an aTc-inducible promoter. dCas12 was induced at 17hpi by adding 5nM aTc to the
616 media. In a control infection, the expression of dCas12 was not induced. Cells were harvested at
617 24hpi and the morphology of *Ct* in induced and uninduced control cells was assessed in 250
618 cells. 3 replicates were performed, and the values shown are the averages of the 3 replicates (A
619 and B). The localization of endogenous FtsK, endogenous PBP2, and endogenous PBP3 was
620 assessed in cells transformed with the pBOMBL-12CRia plasmid that targets *ftsK* or *pbp2*. The
621 localization is shown in coccoid cells where dCas12 expression was (C) uninduced or (D)
622 induced. White bars are 1μm. (E and F) The localization profiles of FtsK, PBP2, and PBP3 were
623 quantified in uninduced and induced cells. 3 replicates were performed, and the values shown are
624 the averages of the 3 replicates.

625 **Figure 5:** Effect of mecillinam on endogenous FtsK, PBP2, and PBP3 localization. (A) HeLa
626 cells were infected with *Ct* and 20μM mecillinam was added to the media at 17hpi. Untreated
627 coccoid cells were included as a control. The cells were harvested at 21hpi and the morphology
628 of MOMP-stained cell was assessed in 200 cells. 3 replicates were performed, and the values
629 shown are the averages of the 3 replicates. (B and C) The localization of endogenous FtsK,
630 endogenous PBP2, and endogenous PBP3 in untreated coccoid or in mecillinam-treated coccoid
631 cells is shown. Bars are1μM. (D and E) Localization of FtsK, PBP2, and PBP3 in untreated and
632 mecillinam-treated coccoid cells was quantified in 50 cells. Three replicates were performed, and
633 the values shown are the averages of the 3 replicates.
634 **Figure 6:** PG distribution in *Ct*. HeLa cells were infected with *Ct* L2. At 17hpi, 4mM ethylene-
635 DA-DA (EDA-DA) was added to the media, the cells were harvested at 21hpi, and the EDA-DA
636 was click labeled and compared to the distribution of MOMP. (A) Imaging analyses revealed
637 that PG formed foci at the septum and at the base in some dividing cells. (B) Imaging analyses
638 revealed that PG organization at the septum and at the base of some dividing cells differed. In
639 this example, a PG foci was detected at the septum and a PG ring was detected at the base of a
640 dividing cell. (C) The localization of click-labeled PG was compared to the localization of
641 endogenous FtsK and mCherry-PBP3 at the septum of dividing cells. 3D projections revealed
642 that multiple foci of each protein are associated with PG intermediates. Cartoons are included to
643 assist the reader in visualizing the angled orientation of PG relative to the MOMP-stained septum
644 in the dividing cells. (D) PG organization in untreated coccoid cells. (E) Quantification of PG
645 organization in untreated coccoid cells, A22-treated coccoid cells, mecillinam-treated coccoid
646 cells, and in coccoid cells resulting from the inducible knockdown of *ftsk*. Fifty cells were
647 counted for each condition. Three replicates were performed and the average from the 3

648 replicates is shown. (F) PG organization in A22-treated and mecillinam-treated coccoid cells, and
649 in coccoid cells resulting from the inducible knockdown of *ftsk* is shown. Bars are 1μm. (G)
650 Putative *Ct* divisome assembly pathway is shown. Proteins characterized in this study are bolded.
651 The ordering of the remaining proteins is based on the assembly of the divisome and elongasome
652 in *E. col*i (Du 2017; Liu 2020).
653 **Supp. Fig. S1:**(A) Lysates were prepared from uninfected HeLa cells and HeLa cells infected
654 with *Ct* L2. At 21hpi, lysates were prepared and characterized by immunoblotting with FtsK-
655 specific antibodies. (B) HeLa cells were infected with *Ct* transformed with the various mCherry
656 fusions used in this study; FtsK-mCherry (molecular mass - 114,664 Da), mCherry-PBP2
657 (molecular mass - 150,842 Da), mCherry-PBP3 (molecular mass - 100,150 Da), or mCherry-
658 MreC (molecular mass - 63,906 Da). The fusions were induced with 10nM aTc at 17hpi. HeLa
659 cells were harvested at 21hpi and lysates were prepared and characterized by immunoblotting
660 analysis with a rabbit polyclonal mCherry antibodies. (C) HeLa cells were infected with *Ct*
661 transformed N-terminal fusions of PBP2 or PBP3. The fusions were induced (+aTc) at17hpi.
662 Controls were not induced (-aTc). The cells were harvested at 21hpi and lysates were prepared as
663 described in the Methods and characterized by immunoblotting analysis with rabbit antibodies
664 raised against peptides derived from chlamydial PBP2 or PBP3. The PBP3 antibody primarily
665 detects a single species with the predicted molecular mass of mCherry-PBP3 in the induced
666 sample. The PBP2 antibody primarily detects a species of ~120kD in the induced sample, which
667 is smaller than the predicted molecular mass of mCherry-PBP2 (~150kD). The failure to detect
668 full length mCherry-PBP2 may be due to the masking of the epitope recognized by the PBP2
669 antibody by the N-terminal mCherry tag in the full-length protein. (D) HeLa cells were infected
670 with *Ct* transformed with mCherry-PBP2 or mCherry-PBP3. The fusions were induced by the

671 addition of 10nM aTc to the media of the infected cells at 19hpi. Infected cells were harvested at
672 21hpi and lysates were prepared and stained with the PBP2 or PBP3 antibodies. The staining
673 with the PBP2 and PBP3 antibodies completely overlaps the mCherry fluorescence from the
674 mCherry-PBP2 and mCherry-PBP3 fusions (Bars are 3μm)

675 **Supp. Fig. S2:** (A) HeLa cells were infected with *Ct* transformed with FtsK-mCherry, mCherry-
676 PBP2, mCherry-PBP3, and mCherry-MreC. The fusions were uninduced or induced by the
677 addition of varying amounts of aTc to the media of the infected cells at 8hpi. The cells were
678 harvested at 48hpi and *Ct* were isolated. The number of infectious *Ct* in the lysates was measured
679 by an IFU assay. Chi-squared analysis revealed that induction of the fusions did not have a
680 statistically significant effect on the growth of *Ct* and the production of infectious EBs. (B) Each
681 of the mCherry fusions accumulate in foci at the septum and in foci at the base (marked with
682 arrowheads) of dividing cells with secondary buds.

683 **Supp. Fig. S3: (A)** Localization analyses with rabbit polyclonal antibodies that recognize
684 endogenous PBP2 or PBP3. These analyses revealed that endogenous PBP2 and PBP3
685 accumulate in foci in coccoid cells, and in foci at the septum, foci at the septum and base, or in
686 foci at the base alone in cell division intermediates in *Ct*. PBP2 and PBP3 foci are also detected
687 at the base of secondary buds. Bars are1μm (B) Quantification revealed that the localization
688 profiles of endogenous PBP2 and PBP3 were not statistically different than the localization
689 profiles of the mCherry-PBP2 and mCherry-PBP3 fusions shown in Fig. 2C.

690 **Supp. Fig. S4:** HeLa cells were infected with *Ct* transformed with PBP2, PBP3, or MreC with an
691 N-terminal mCherry tag, or with *Ct* transformed with an MreB_6xHis fusion (Lee 2020). Each of
692 the fusions was induced by adding 10nM aTc to the media at 17hpi. Lysates were prepared at
693 21hpi and the cells were fixed and stained with a MOMP antibody. The distribution of the

694 mCherry fluorescence in dividing cells that had not initiated secondary bud formation is shown.
695 Cells expressing the MreB_6xHis fusion were stained with rabbit anti-6xHis antibody (red) and
696 MOMP antibodies (green). In the dividing cells shown there are (A) foci of the fusions at the
697 septum and at the base of the mother cell or foci at the base of the mother cell only that overlap
698 the distribution of FtsK. Bars are1μm (B) The percentage of dividing cells in which the fusions
699 overlapped the distribution of FtsK at the septum, at the septum and at the base, and at the base
700 alone was quantified in 100 cells. Three independent replicates were performed and the values
701 shown are the average of the 3 replicates.
702 **Supp. Fig. S5:** HeLa cells were infected with *Ct* transformed with the pBOMBL12CRia
703 plasmid that constitutively expresses *ftsK* or *pbp2*-targeting crRNAs. dCas12 expression was
704 induced by the addition of 5nM aTc to the media of infected cells at 8hpi. Control cells were not
705 induced. Nucleic acids were isolated from induced cells and from uninduced controls at various
706 times post-infection, and RT-qPCR was used to measure *ftsK* or *pbp2* transcript levels. (A) The
707 induction of dCas12 resulted in ~10-fold reduction in *ftsK* transcript levels in cells expressing the
708 *ftsK*-targeting crRNA, (B) and ~8-fold reduction in *pbp2* transcript levels in cells expressing the
709 *pbp2*-targeting crRNA, while these crRNAs had minimal or no effect on chlamydial *euo* and
710 *omcB* transcript levels. HeLa cells were infected with *Ct* transformed pBOMBL12CRia plasmid
711 that constitutively expresses a (C) *ftsK* or (D) *pbp2*-targeting crRNA. dCas12 expression was
712 induced by the addition of 5nM aTc to the media of infected cells at 8hpi. Control cells were not
713 induced. The infected cells were fixed at 24hpi and stained with MOMP and Cas12 antibodies.
714 *Ct* morphology was normal and dCas12 was undetectable in the inclusions of uninduced control
715 cells. Foci of dCas12 were observed in induced cells, and *Ct* in the inclusion exhibited an
716 enlarged aberrant morphology. Bars in C and D are 2μm. (E) HeLa cells were infected with *Ct*

717 transformed with the pBOMBL12CRia plasmid that constitutively expresses a *ftsK* or *pbp2*-
718 targeting crRNA. dCas12 was induced at 17hpi by the addition of 10nM aTc to the media.
719 Control cells were not induced. The cells were harvested at 21hpi, and *Ct* were prepared and
720 stained with antibodies that recognize that endogenous FtsK or PBP2. Quantification shows that
721 polarized foci of FtsK and PBP2 were almost undetectable when *ftsK* or *pbp2* were transiently
722 knocked down.
723 **Supp. Fig. S6**. MreC rings in (A) dividing *Ct* and in (B) coccoid *Ct*. Bars are1μm.
724 **Supp. Table S1** List of primers and plasmids used for cloning mCherry fusions of FtsK, PBP2,
725 PBP3, MreB and MreC.
726 **Supp. Table S2**: List of primers used for RT-qPCR.
727 **References:**
728 **Abdelrahman, Y., Ouellette, Scot P., Belland, Robert J., Cox, John V. (2016). "Polarized**
729 **Cell Division of Chlmaydia Trachomatis " PLOS Pathogens**
730 +
731 **Abdelrahman, Y. M. and R. J. Belland (2005). "The chlamydial developmental cycle."**
732 **FEMS Microbiol Rev 29(5): 949-959.**
733
734 **Abdelrahman, Y. O., Scot P. Belland, Robert J. Cox, John V. (2016). "Polarized Cell**
735 **Division of Chlamydia trachomatis." PLOS Pathogens.**
736
737 **F. Barre, B. Søballe, B. Michel, M. Aroyo, M. Robertson, D. Sherratt, Circles: The**
738 **replication-recombination-chromosome segregation connection, Proc. Natl. Acad. Sci.**
739 **U.S.A. 98 (15) 8189-8195, https://doi.org/10.1073/pnas.111008998 (2001).**

740

741 **Barrows, J. M. and E. D. Goley (2021). "FtsZ dynamics in bacterial division: What, how,**

742 **and why?" Curr Opin Cell Biol 68: 163-172.**

743

744 **Bean, G. J., S. T. Flickinger, W. M. Westler, M. E. McCully, D. Sept, D. B. Weibel and K.**

745 **J. Amann (2009). "A22 disrupts the bacterial actin cytoskeleton by directly binding and**

746 **inducing a low-affinity state in MreB." Biochemistry 48(22): 4852-4857.**

747

748 **Bisson-Filho, A. W., Y. P. Hsu, G. R. Squyres, E. Kuru, F. Wu, C. Jukes, Y. Sun, C.**

749 **Dekker, S. Holden, M. S. VanNieuwenhze, Y. V. Brun and E. C. Garner (2017).**

750 **"Treadmilling by FtsZ filaments drives peptidoglycan synthesis and bacterial cell**

751 **division." Science 355(6326): 739-743.**

752

753 **Blakely, G., May, G., McCulloch, R., Arciszewska, L. K., Burke, M., Lovett, S. T., &**

754 **Sherratt, D. J. (1993). Two related recombinases are required for site-specific**

755 **recombination at dif and cer in E. coli K12. *Cell*, *75*(2), 351–361.**

756 **https://doi.org/10.1016/0092-8674(93)80076-q**

757

758 **Cox, J. V. A., Yasser Mohamed. Ouellette, Scot P. (2020). "Penicillin-binding proteins**

759 **regulate multiple steps in the polarized cell division process of Chlamydia." Nature**

760 **Du, S. L., Joe (2017). "Assembly and activation of the Escherichia coli divisome."**

761 **Molecular Microbiology.**

762

763 **GW, L. (2021). "Localized Peptidoglycan Biosynthesis in Chlamydia trachomatis**
764 **Conforms to the Polarized Division and Cell Size Reduction Developmental Models." Front**
765 **Microbiol.**
766
767 **Kaur, H. and A. M. Lynn (2022). "Mapping the FtsQBL divisome components in bacterial**
768 **NTD pathogens as potential drug targets." Front Genet 13: 1010870.**
769
770 **Kemege, K. E., J. M. Hickey, M. L. Barta, J. Wickstrum, N. Balwalli, S. Lovell, K. P.**
771 **Battaile and P. S. Hefty (2015). "Chlamydia trachomatis protein CT009 is a structural and**
772 **functional homolog to the key morphogenesis component RodZ and interacts with division**
773 **septal plane localized MreB." Mol Microbiol 95(3): 365-382.**
774
775 **Kocaoglu, O., H. C. Tsui, M. E. Winkler and E. E. Carlson (2015). "Profiling of β-lactam**
776 **selectivity for penicillin-binding proteins in Streptococcus pneumoniae D39." Antimicrob**
777 **Agents Chemother 59(6): 3548-3555.**
778
779 **Lee, J., Cox, John V., Ouellette, Scot P. (2020). "Critical Role for the Extended N Terminus**
780 **of Chlmaydial MreB in Directing Its Membrane Association and Potential Interaction with**
781 **Divisome Proteins " Journal of Bacteriology 202.**
782
783 **Lee, J. K., G. A. Enciso, D. Boassa, C. N. Chander, T. H. Lou, S. S. Pairawan, M. C. Guo,**
784 **F. Y. M. Wan, M. H. Ellisman, C. Sütterlin and M. Tan (2018). "Replication-dependent**

785 **size reduction precedes differentiation in Chlamydia trachomatis." Nature**
786 **Communications 9(1): 45.**
787
788 **Liechti, G., E. Kuru, M. Packiam, Y. P. Hsu, S. Tekkam, E. Hall, J. T. Rittichier, M.**
789 **VanNieuwenhze, Y. V. Brun and A. T. Maurelli (2016). "Pathogenic Chlamydia Lack a**
790 **Classical Sacculus but Synthesize a Narrow, Mid-cell Peptidoglycan Ring, Regulated by**
791 **MreB, for Cell Division." PLoS Pathog 12(5): e1005590.**
792
793 **Liechti, G. W., E. Kuru, E. Hall, A. Kalinda, Y. V. Brun, M. VanNieuwenhze and A. T.**
794 **Maurelli (2014). "A new metabolic cell-wall labelling method reveals peptidoglycan in**
795 **Chlamydia trachomatis." Nature 506(7489): 507-510.**
796
797 **Liu, X. B., Jacob. Consoli, Elisa. Vollmer, Waldemar. Blaauwen, Tanneke den. (2020).**
798 **"MreC and MreD balance the interaction between the elongasome proteins PBP2 and**
799 **RodA." PLOS Genetics.**
800
801 **Massey, T. H., Mercogliano, C. P., Yates, J., Sherratt, D. J., & Löwe, J. (2006). Double-**
802 **stranded DNA translocation: structure and mechanism of hexameric FtsK. *Molecular***
803 ***cell*, *23*(4), 457–469. https://doi.org/10.1016/j.molcel.2006.06.019**
804
805 **Ouellette, S. P., E. A. Blay, N. D. Hatch and L. A. Fisher-Marvin (2021). "CRISPR**
806 **Interference To Inducibly Repress Gene Expression in Chlamydia trachomatis." Infect**
807 **Immun 89(7): e0010821.**

808

809 **Ouellette SP, F.-M. L., Harpring M, Lee J, Rucks EA, Cox JV (2022). "Localized**
810 **cardiolipin synthesis is required for the assembly of MreB during the polarized cell division**
811 **of Chlamydia trachomatis." PLOS Pathogens.**

812

813 **Ouellette SP, K. G., Subtil A, Ladant D. (2012). "Chlamydia co-opts the rod shape-**
814 **determining proteins MreB and Pbp2 for cell division." Mol Microbiol.**

815

816 **Ouellette, S. P., K. J. Rueden, Y. M. AbdelRahman, J. V. Cox and R. J. Belland (2015).**
817 **"Identification and Partial Characterization of Potential FtsL and FtsQ Homologs of**
818 **Chlamydia." Front Microbiol 6: 1264.**

819

820 **Ouellette, S. P., K. J. Rueden, E. Gauliard, L. Persons, P. A. de Boer and D. Ladant (2014).**
821 **"Analysis of MreB interactors in Chlamydia reveals a RodZ homolog but fails to detect an**
822 **interaction with MraY." Front Microbiol 5: 279.**

823

824 **Ouellette, S. P. L., Junghoon. Cox, John V. (2020). "Division without Binary Fission: Cell**
825 **Division in the FtsZ-Less Chlamydia." Journal of Bacteriology.**

826

827 **Ouellette, S. P. R., Kelsey J. AbdelRahman, Yasser M. Cox, John V. Belland, Robert J.**
828 **(2015). "Identification and Partial Characterization of Potential FtsL and FtsQ Homologs**
829 **of Chlamydia." Frontiers in Microbiology.**

830

831 **Rivas-Marín, E., I. Canosa, E. Santero and D. P. Devos (2016). "Development of Genetic**
832 **Tools for the Manipulation of the Planctomycetes." Front Microbiol 7: 914.**
833
834 **Rivas-Marin, E., D. Moyano-Palazuelo, V. Henriques, E. Merino and D. P. Devos (2023).**
835 **"Essential gene complement of Planctopirus limnophila from the bacterial phylum**
836 **Planctomycetes." Nat Commun 14(1): 7224.**
837
838 **Stephens, C. (1998). "Bacterial sporulation: a question of commitment?" Curr Biol 8(2):**
839 **R45-48.**
840
841 **Veiga, H. and M. G. Pinho (2017). "Staphylococcus aureus requires at least one**
842 **FtsK/SpoIIIE protein for correct chromosome segregation." Mol Microbiol 103(3): 504-**
843 **517.**
844
845 **Wang, T. J., P. Gona, M. G. Larson, G. H. Tofler, D. Levy, C. Newton-Cheh, P. F. Jacques,**
846 **N. Rifai, J. Selhub, S. J. Robins, E. J. Benjamin, R. B. D'Agostino and R. S. Vasan (2006).**
847 **"Multiple biomarkers for the prediction of first major cardiovascular events and death." N**
848 **Engl J Med 355(25): 2631-2639.**
849
850 **Wang, Y., S. Kahane, L. T. Cutcliffe, R. J. Skilton, P. R. Lambden and I. N. Clarke (2011).**
851 **"Development of a transformation system for Chlamydia trachomatis: restoration of**
852 **glycogen biosynthesis by acquisition of a plasmid shuttle vector." PLoS Pathog 7(9):**
853 **e1002258.**

854

855 **Wiegand, S., M. Jogler, C. Boedeker, D. Pinto, J. Vollmers, E. Rivas-Marín, T. Kohn, S. H.**
856 **Peeters, A. Heuer, P. Rast, S. Oberbeckmann, B. Bunk, O. Jeske, A. Meyerdierks, J. E.**
857 **Storesund, N. Kallscheuer, S. Lücker, O. M. Lage, T. Pohl, B. J. Merkel, P. Hornburger, R.**
858 **W. Müller, F. Brümmer, M. Labrenz, A. M. Spormann, H. J. M. Op den Camp, J.**
859 **Overmann, R. Amann, M. S. M. Jetten, T. Mascher, M. H. Medema, D. P. Devos, A. K.**
860 **Kaster, L. Øvreås, M. Rohde, M. Y. Galperin and C. Jogler (2020). "Cultivation and**
861 **functional characterization of 79 planctomycetes uncovers their unique biology." Nat**
862 **Microbiol 5(1): 126-140.**
863

864 **Yang, X., Z. Lyu, A. Miguel, R. McQuillen, K. C. Huang and J. Xiao (2017). "GTPase**
865 **activity-coupled treadmilling of the bacterial tubulin FtsZ organizes septal cell wall**
866 **synthesis." Science 355(6326): 744-747.**
867

868 **Yu, X. C., A. H. Tran, Q. Sun and W. Margolin (1998). "Localization of cell division**
869 **protein FtsK to the Escherichia coli septum and identification of a potential N-terminal**
870 **targeting domain." J Bacteriol 180(5): 1296-1304.**
871
872

Figure 1

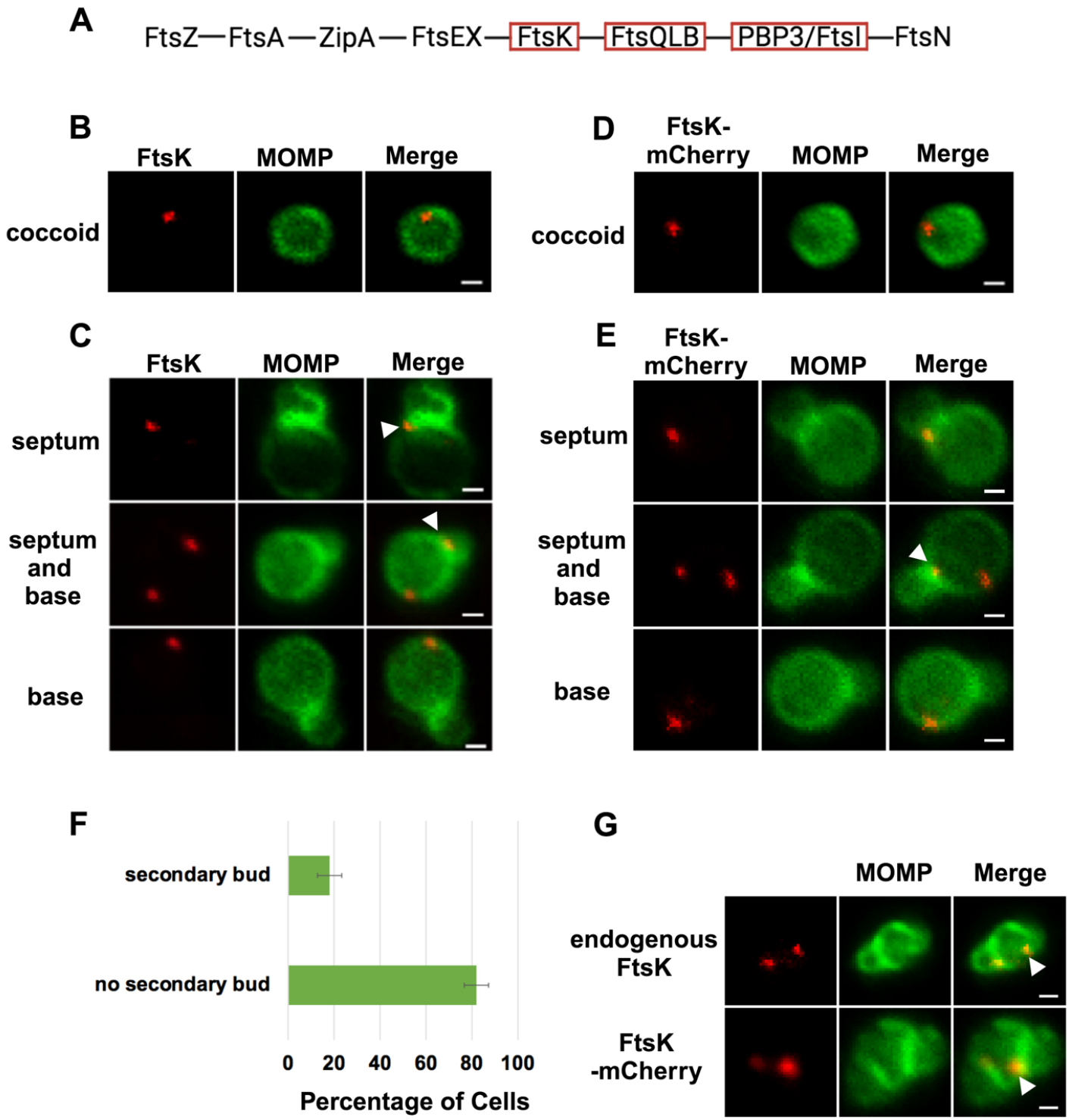
A
FtsZ—FtsA—ZipA—FtsEX—FtsK—FtsQLB—PBP3/FtsI—FtsN
B
FtsK
MOMP
Merge
coccoid
C
FtsK
MOMP
Merge
septum
septum and base
base
D
FtsK-mCherry
MOMP
Merge
coccoid
E
FtsK-mCherry
MOMP
Merge
septum
septum and base
base
F
secondary bud
no secondary bud
0
20
40
60
80
100
Percentage of Cells
G
MOMP
Merge
endogenous FtsK
FtsK -mCherry

Figure 2

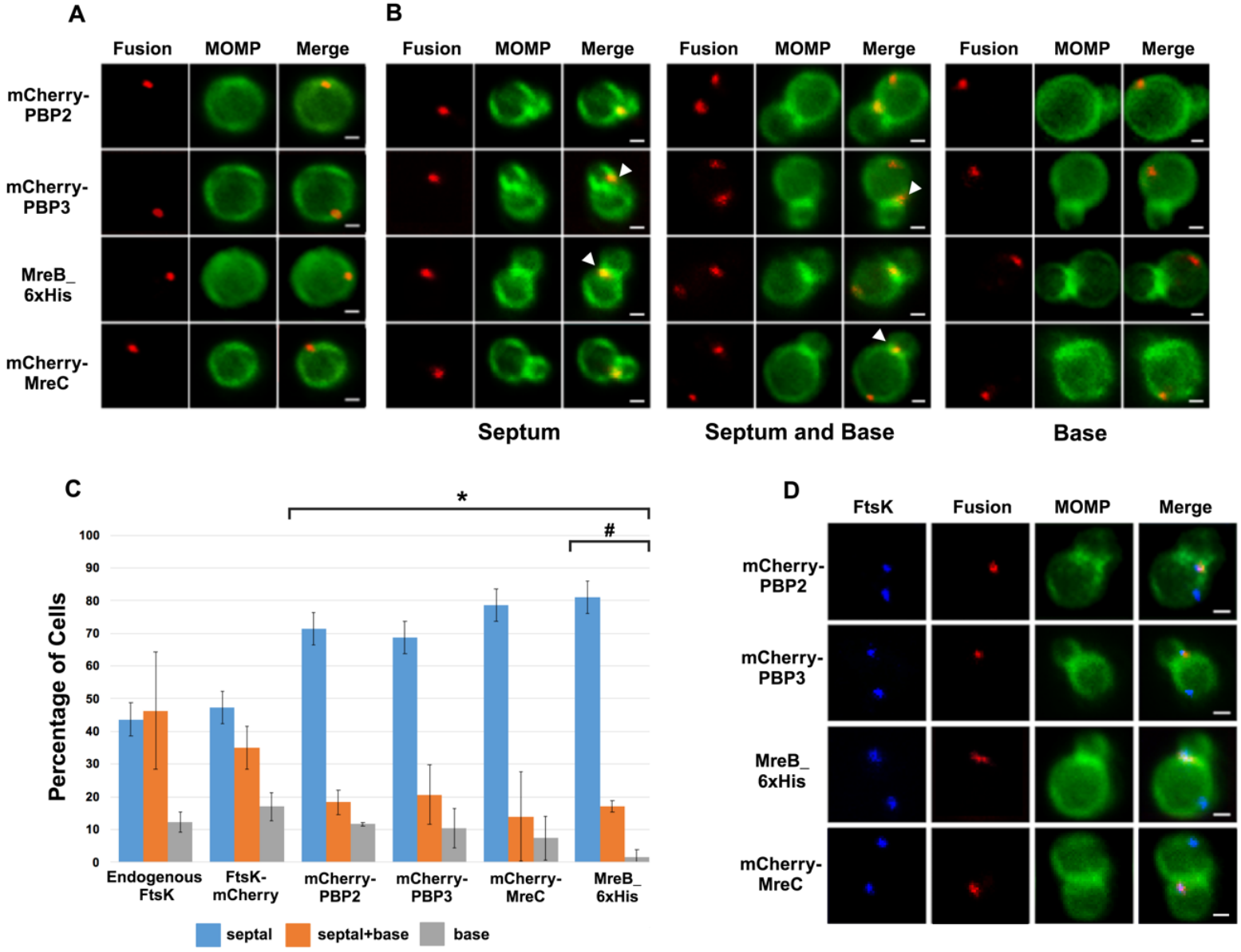
A
B
Fusion
MOMP
Merge
mCherry-PBP2
mCherry-PBP3
MreB_6xHis
mCherry-MreC
Septum
Septum and Base
Base
C
Percentage of Cells
100
90
80
70
60
50
40
30
20
10
0
*
#
Endogenous FtsK
FtsK-mCherry
mCherry-PBP2
mCherry-PBP3
mCherry-MreC
MreB_6xHis
septal
septal+base
base
D
FtsK
Fusion
MOMP
Merge
mCherry-PBP2
mCherry-PBP3
MreB_6xHis
mCherry-MreC

Figure 3

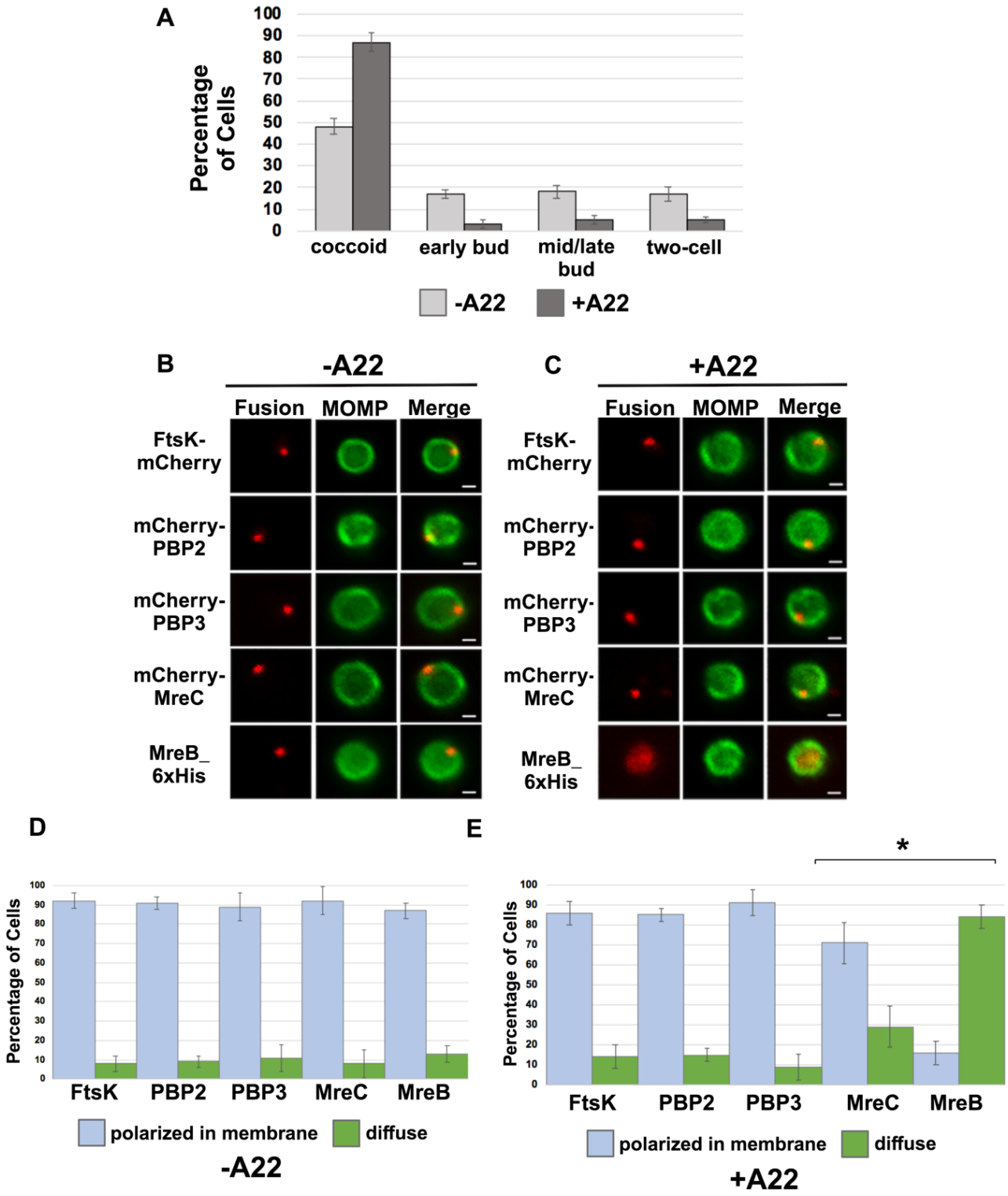
A
Percentage of Cells
100
90
80
70
60
50
40
30
20
10
0
coccoid
early bud
mid/late bud
two-cell
-A22
+A22
B
-A22
Fusion
MOMP
Merge
FtsK-mCherry
mCherry-PBP2
mCherry-PBP3
mCherry-MreC
MreB_6xHis
C
+A22
Fusion
MOMP
Merge
FtsK-mCherry
mCherry-PBP2
mCherry-PBP3
mCherry-MreC
MreB_6xHis
D
Percentage of Cells
FtsK
PBP2
PBP3
MreC
MreB
polarized in membrane
diffuse
-A22
E
*
Percentage of Cells
FtsK
PBP2
PBP3
MreC
MreB
polarized in membrane
diffuse
+A22

Figure 4

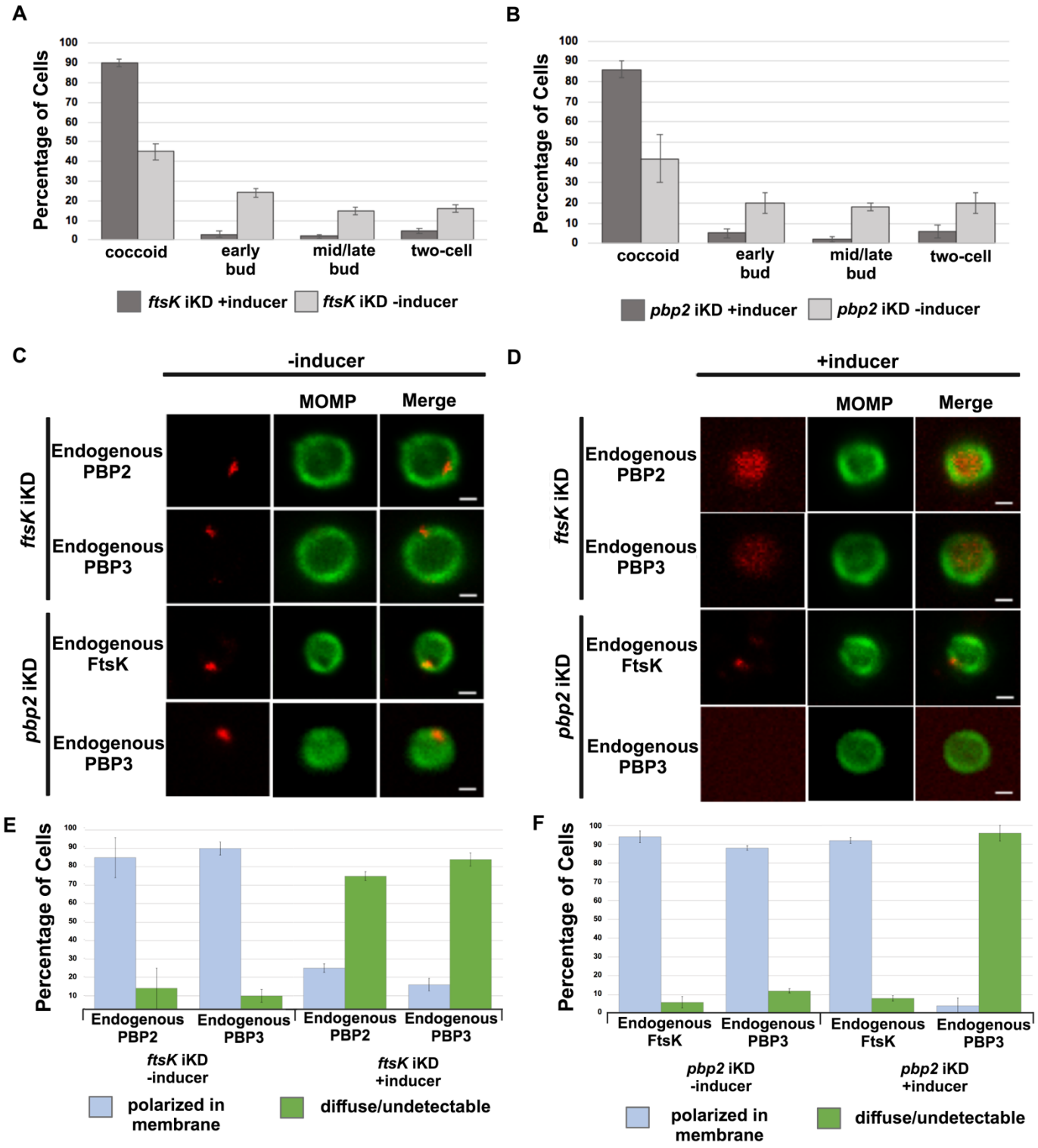
A
Percentage of Cells
100
90
80
70
60
50
40
30
20
10
0
coccoid
early bud
mid/late bud
two-cell
ftsK iKD +inducer
ftsK iKD -inducer
B
Percentage of Cells
coccoid
early bud
mid/late bud
two-cell
pbp2 iKD +inducer
pbp2 iKD -inducer
C
-inducer
MOMP
Merge
ftsK iKD
Endogenous PBP2
Endogenous PBP3
pbp2 iKD
Endogenous FtsK
Endogenous PBP3
D
+inducer
MOMP
Merge
ftsK iKD
Endogenous PBP2
Endogenous PBP3
pbp2 iKD
Endogenous FtsK
Endogenous PBP3
E
Percentage of Cells
Endogenous PBP2
Endogenous PBP3
Endogenous PBP2
Endogenous PBP3
ftsK iKD -inducer
ftsK iKD +inducer
polarized in membrane
diffuse/undetectable
F
Percentage of Cells
Endogenous FtsK
Endogenous PBP3
Endogenous FtsK
Endogenous PBP3
pbp2 iKD -inducer
pbp2 iKD +inducer
polarized in membrane
diffuse/undetectable

Figure 5

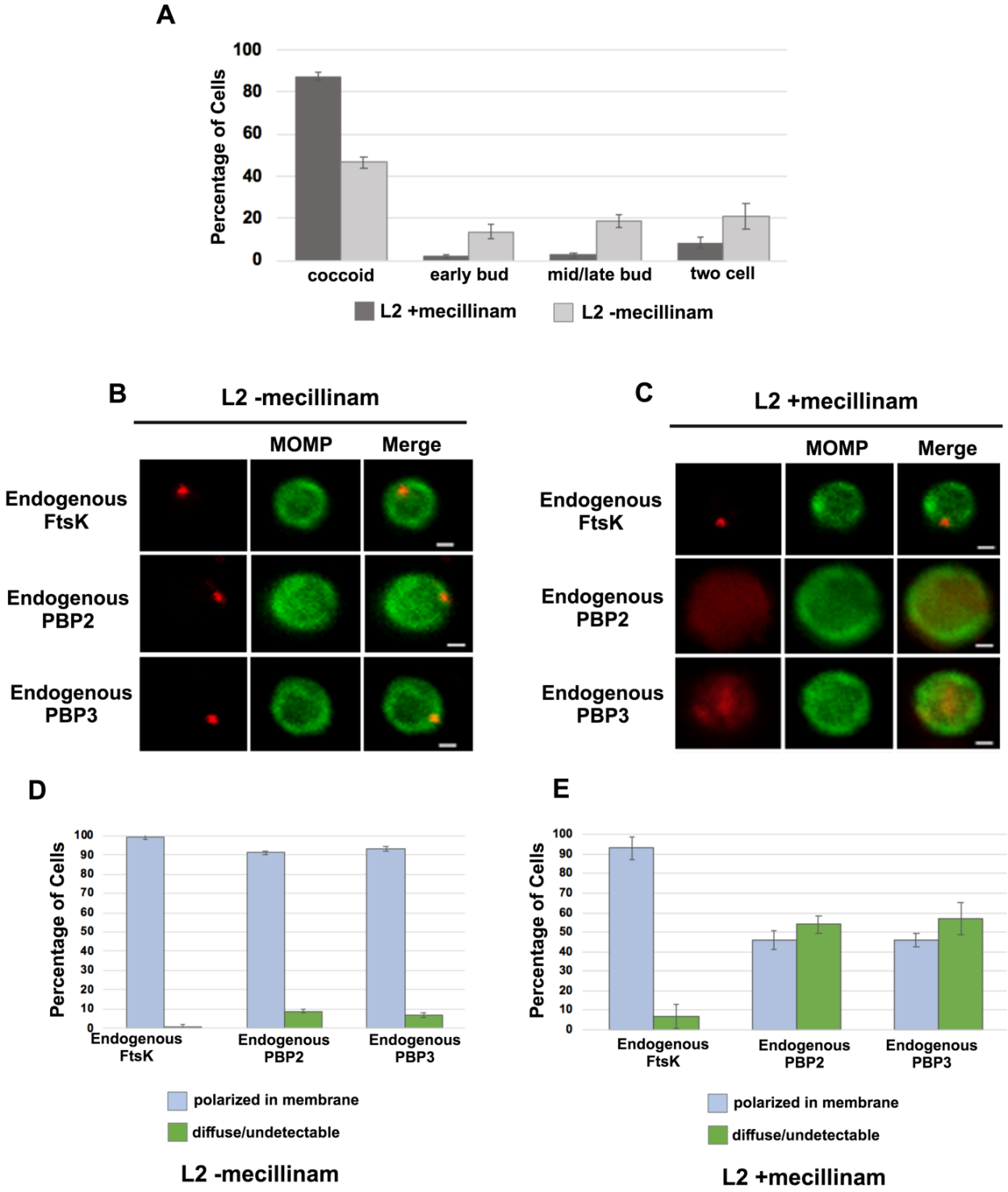
A
Percentage of Cells
100
80
60
40
20
0
coccoid
early bud
mid/late bud
two cell
L2 +mecillinam
L2 -mecillinam
B
L2 -mecillinam
MOMP
Merge
Endogenous FtsK
Endogenous PBP2
Endogenous PBP3
C
L2 +mecillinam
MOMP
Merge
Endogenous FtsK
Endogenous PBP2
Endogenous PBP3
D
Percentage of Cells
100
90
80
70
60
50
40
30
20
10
0
Endogenous FtsK
Endogenous PBP2
Endogenous PBP3
polarized in membrane
diffuse/undetectable
L2 -mecillinam
E
Percentage of Cells
100
90
80
70
60
50
40
30
20
10
0
Endogenous FtsK
Endogenous PBP2
Endogenous PBP3
polarized in membrane
diffuse/undetectable
L2 +mecillinam

Figure 6

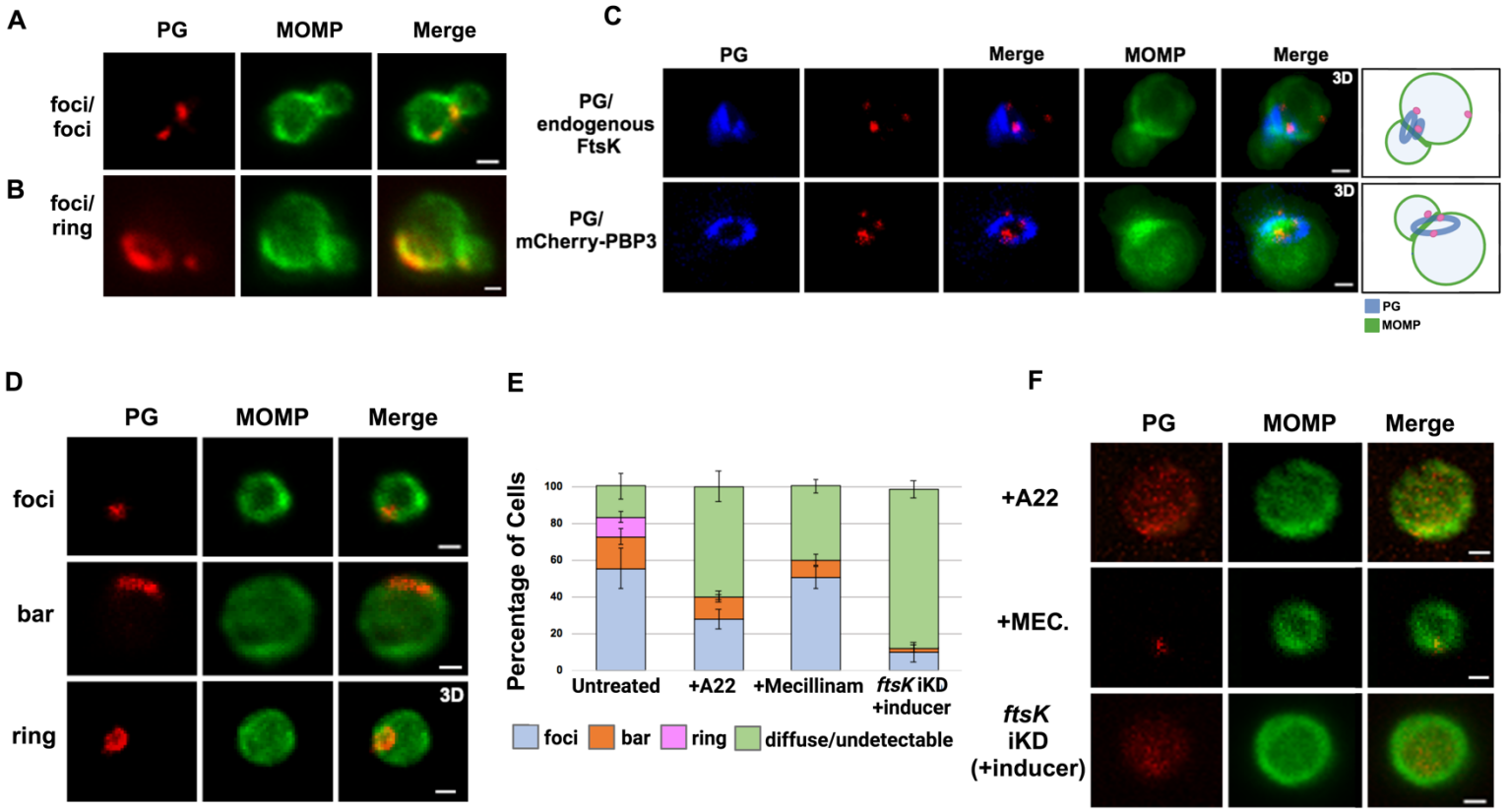

G

FtsK — FtsQLB — RodA — **PBP2** — FtsW — **PBP3** — **MreC** — **MreB** — RodZ

Supp. Figure S1

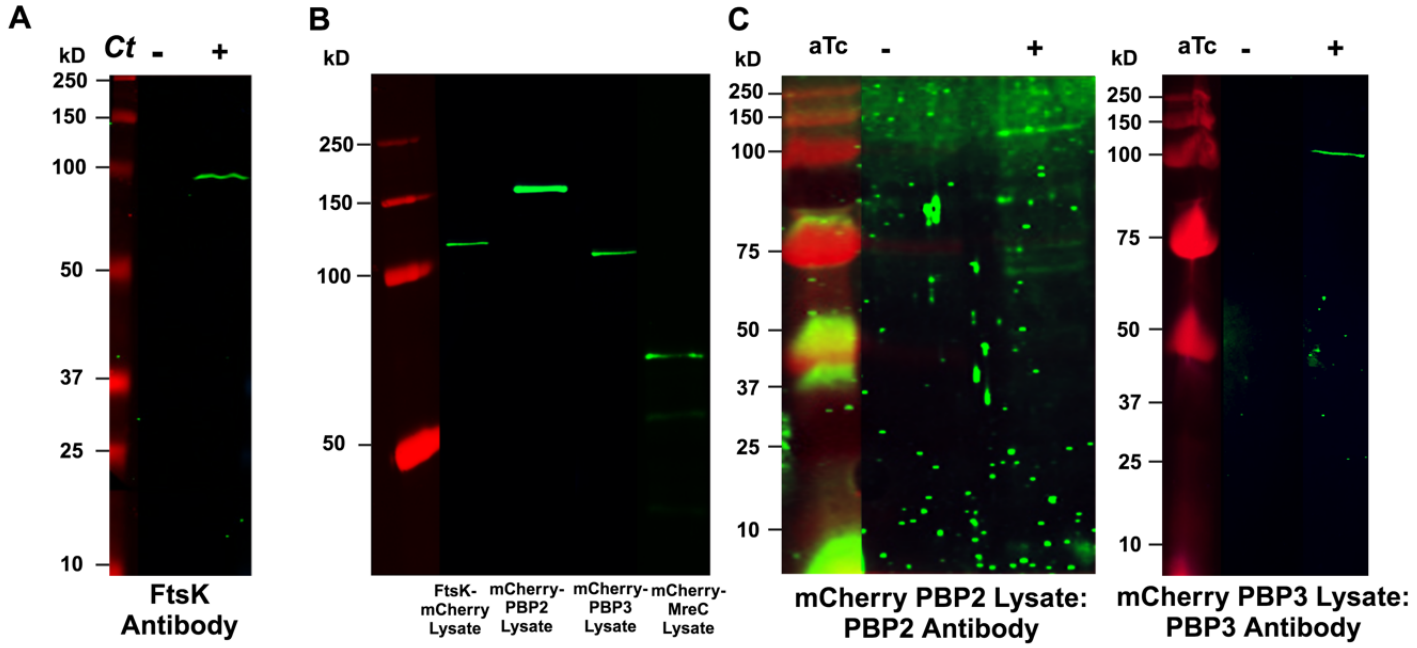

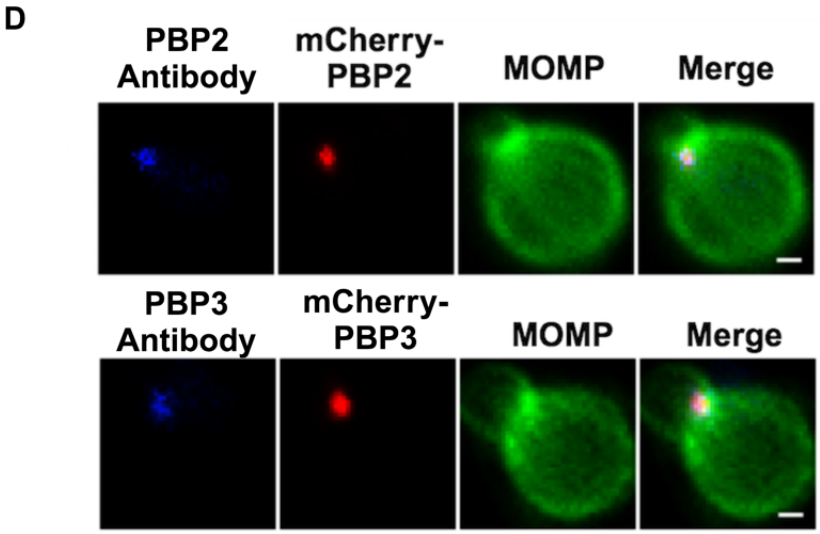

Supp. Figure S2

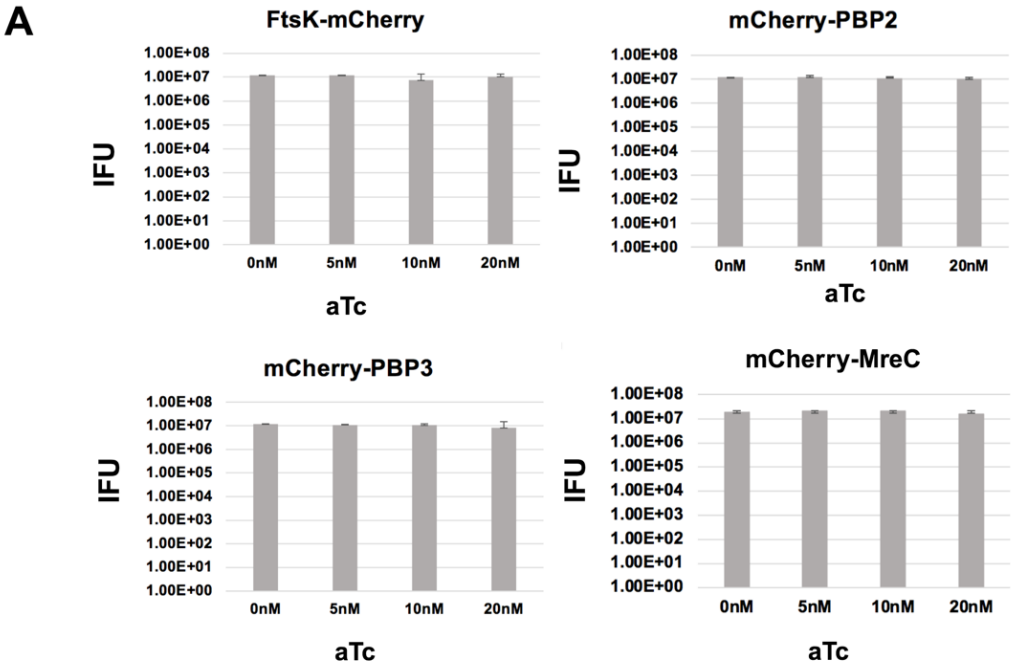

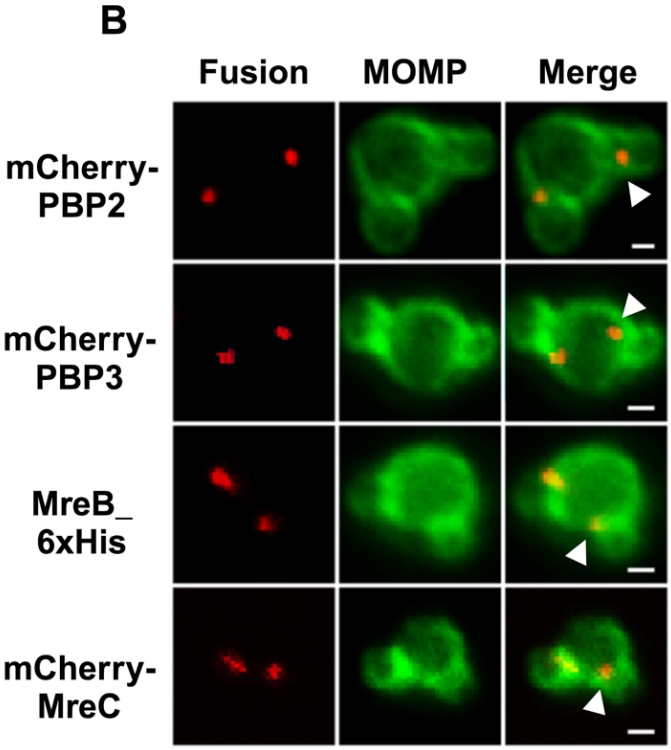

Supp. Figure S3

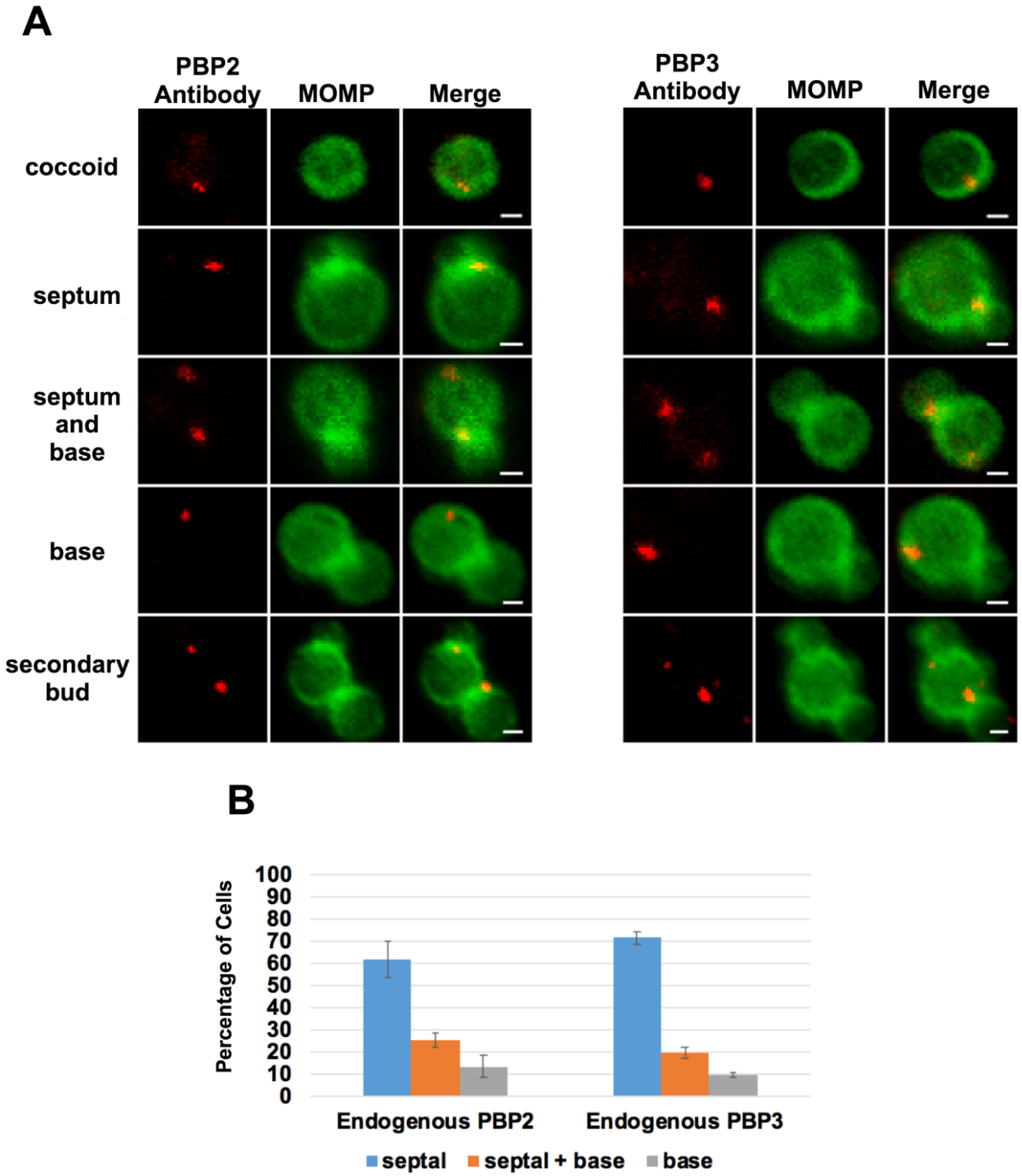

Supp. Figure S4

A

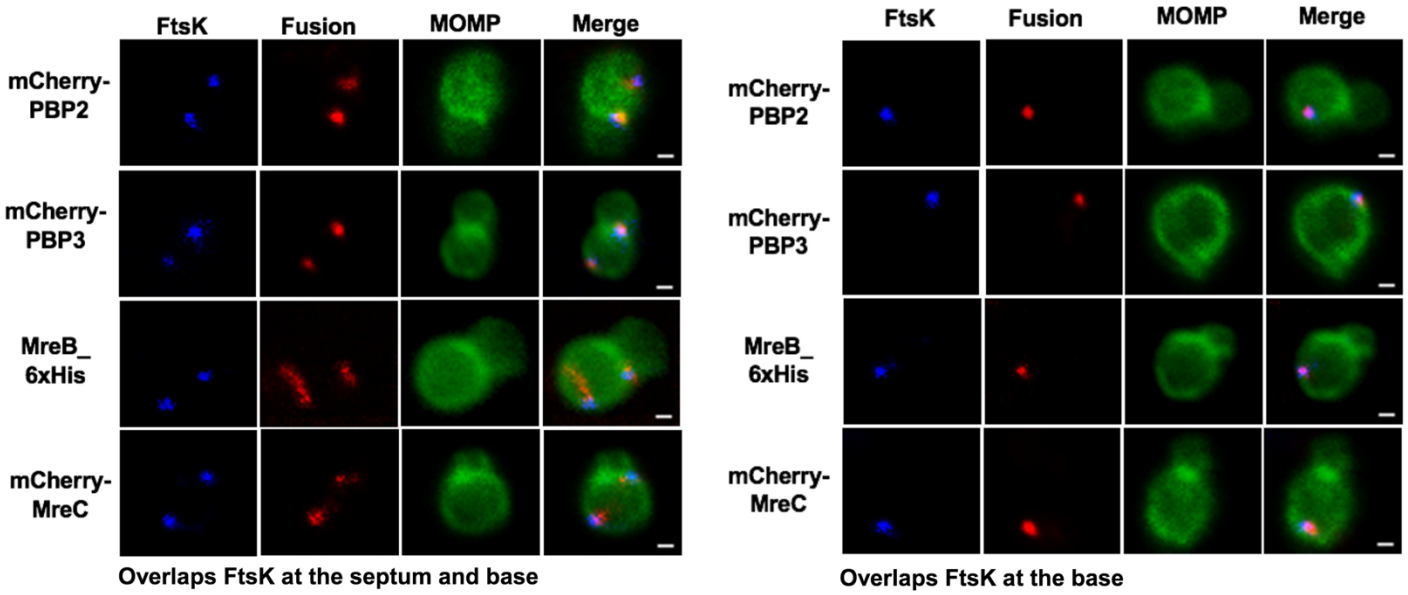

B

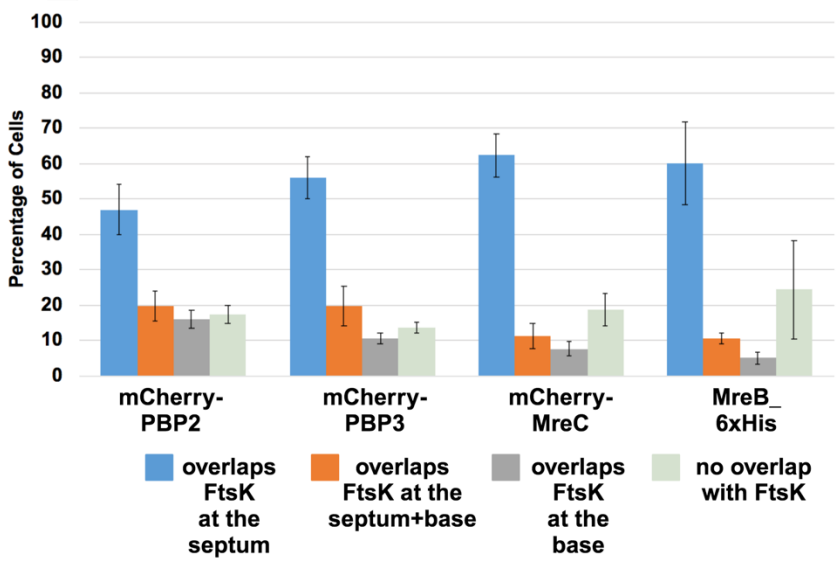

Supp. Figure S5

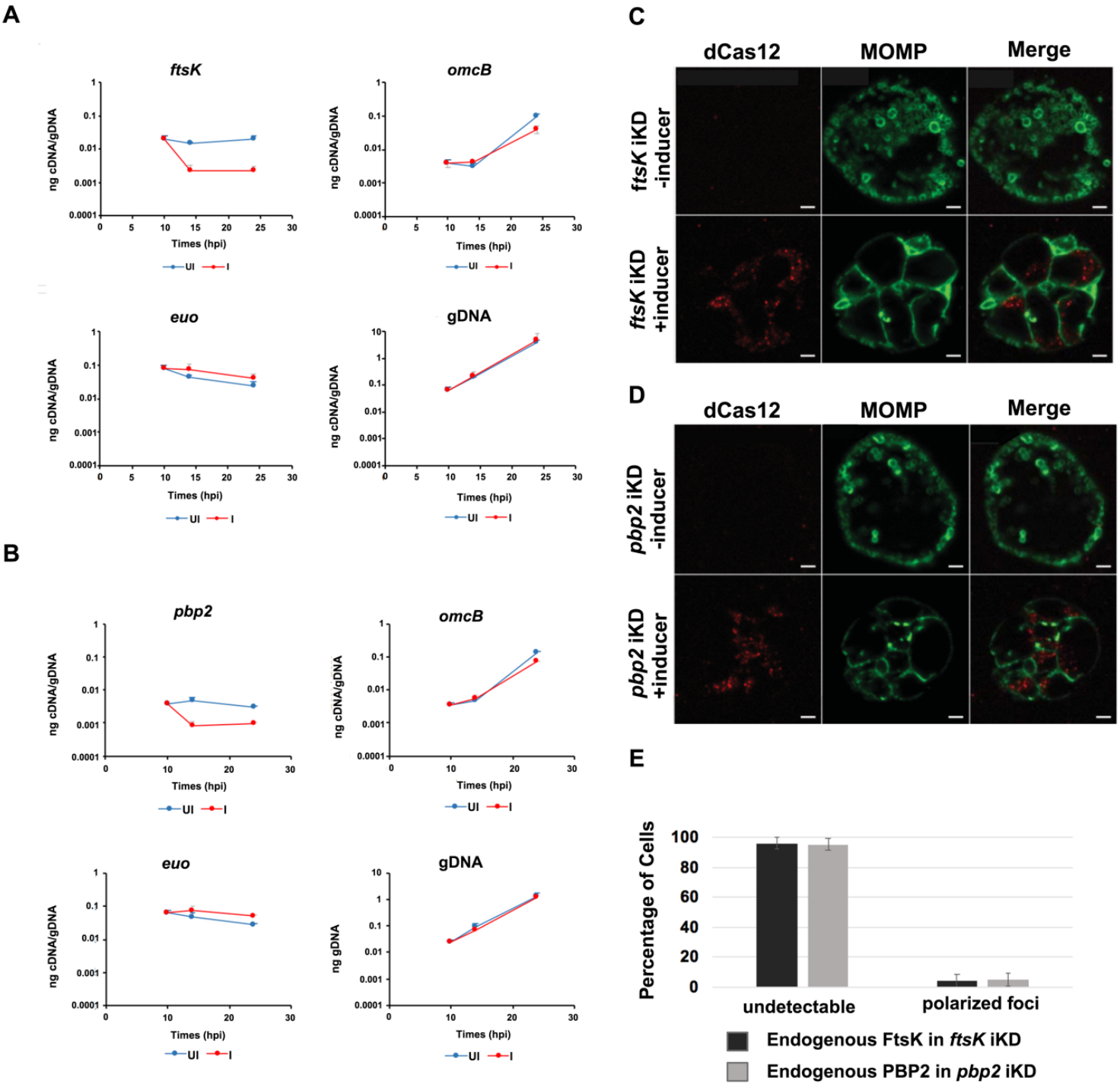

Supp. Figure S6

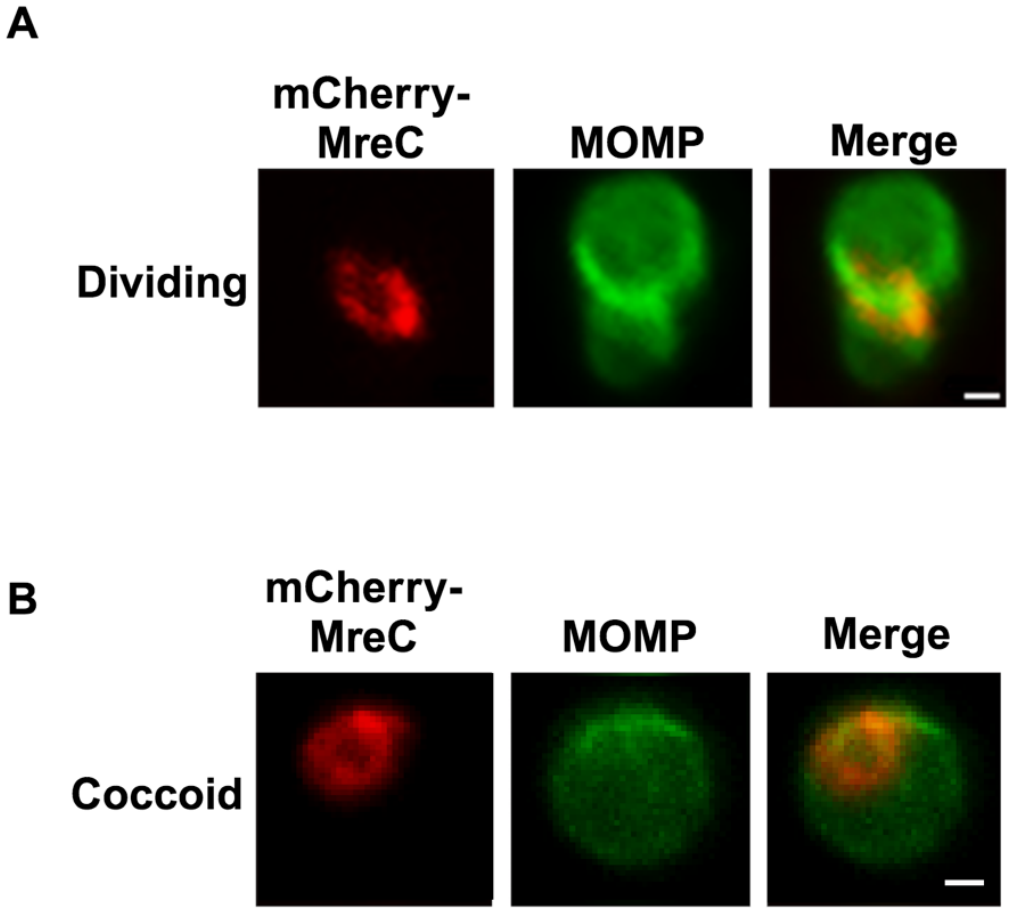

Supp. Table S1

Primer Name	Primer Sequence (5'-3')	GC content (%)	TM (°C)
FtsK_mCherry (fwd)	AGAGGAGAAAGGATCTGCGGCCGCATGGGAAAAGAACGGAAGAAAGCAAG	52	72.8
FtsK_mCherry (rvs)	CCCTTAGAGACCATTGCGGCCGCATCGTCCTGATTTGATAATTGGACTAGTATTTGAC	47	72.4
mCherry_PBP2 (fwd)	ATGGTCTCTAAGGGCGAGGAAGAC	54	59.1
mCherry_PBP2 (rvs)	ATGGTCGACCGGTACCTTAGCTGAAAGATTTTTTACGAATCTCTTCCCATTTCTCTATC	41	70.2
mCherry_PBP3 (fwd)	ATGGTCTCTAAGGGCGAGGAAGAC	54	59.1
mCherry_PBP3 (rvs)	ATGGTCGACCGGTACCCTATTTGCGATTCCATTCCTCATATAGCAG	48	69.9
mCherry_MreC (fwd)	ATGGTCTCTAAGGGCGAGGAAGAC	54	59.1
mCherry_MreC (rvs)	ATGGTCGACCGGTACCCTACTCCCAAATCAAACCAAAAATATCAGGACG	47	70.4
Plasmid	pBOMB4-tet		

Supp. Table S2

Primer Name	Primer Sequence (5'-3')	GC content (%)	TM (°C)
ftsK (fwd)	CGACTCCAAGTTCCTCTTCTTC	39.1	55.2
ftsK (rvs)	GATCCAGTGGTTCCTGCAATA	47.6	54.6
pbp2 (fwd)	TAACACTGACGCGGAACATAG	47.6	55.1
pbp2 (rvs)	CCGAAAGCATGAGCAGATAGA	47.6	54.8
omcB (fwd)	CGGTAGGATCTCCCTATCCTATT	47.8	54.4
omcB (rvs)	CGAACTCTGCTTCACATGGTA	47.6	55
euo (fwd)	CGAAGACTACTCGTTGGGAAATA	43.5	54.7
euo (rvs)	AACAGAAGCTCTCCTTGATAAGT	39.1	53.8